 CMES, vol.42, no.3, pp.217-256, 2009

Extended Limit Analysis of Strain Softening Frames Involving 2nd-Order Geometric Nonlinearity and Limited Ductility

S. Tangaramvong[1] **and F. Tin-Loi**[1]

Abstract: Classical limit analysis is extended to include the effects of 2nd-order geometric and material nonlinearities, as well as the inclusion of limited ductility constraints. For the class of frame structures considered, the material constitutive model adopted can simultaneously accommodate the effects of combined axial and flexural force as well as local softening instability through the use of piecewise linearized yield surfaces. The main feature of the approach developed is to compute, in a single step, an upper bound to the maximum load. Corresponding displacements and stresses can be obtained as a by-product of the analysis. The problem is formulated as an instance of the challenging class of so-called mathematical programs with equilibrium constraints (MPECs). A number of numerical examples are provided to validate the robustness and efficiency of the current approach, and to illustrate some key mechanical features expected of realistic frames that exhibit local softening behavior and geometric nonlinearity.

Keywords: Complementarity problem, geometric nonlinearity, limit analysis, limited ductility, material nonlinearity, nonconvex optimization

1 Introduction

There is no doubt that incrementally based analyses, e.g. Maier (1971); Bolzon and Tin-Loi (1999); Cocchetti and Maier (2003); Tangaramvong and Tin-Loi (2007a), which follow the evolution of structures under a given load regime can provide a complete and rich spectrum of the possible structural responses. Such step-by-step elastoplastic analyses can predict accurately the behavior of structural systems that involve both material and geometric nonlinearities (see e.g. DeDonato and Maier (1972); DeFreitas and LloydSmith (1984–85); Tangaramvong and Tin-Loi (2007a); Tonković, Sorić, and Skozrit (2008)), as well as damaging or fracture

[1] School of Civil and Environmental Engineering, The University of New South Wales, Sydney, NSW 2052, Australia.

interfaces [Bolzon and Corigliano (1997); Long, Liu, and Li (2008)]. However, in the presence of strain softening coupled with geometrically nonlinear effects, such evolutive analyses are typically computationally demanding, especially when multiple equilibrium paths exist. For large-size softening structures exhibiting such mechanically crucial phenomena as bifurcation and loss of overall stability, it is not straightforward to capture all solutions, let alone trace the critical equilibrium path. This, it must be noted, is different to the case of traditional (stable) perfect or hardening plasticity for which various robust and efficient numerical techniques, e.g. Maier (1970); DeDonato and Maier (1972); Franchi and Cohn (1980), are well established and can be used.

The importance of including material nonlinearity (e.g. "work-softening" as is considered in this paper) in any structural analysis is well-known. For instance, when any reinforced concrete member is simultaneously subjected to bending and sufficiently high axial compression, compressive fracture can occur, and this leads to a postpeak softening behavior. Examples are prestressed concrete beams, columns loaded by heavy axial forces and frames or arches with high thrusts. Softening behavior can also occur in over-reinforced concrete sections, such as those retrofitted with a fibre laminate bonded on the tensile face of the damaged reinforced concrete beam. Even though the stress-strain relation of steel does not exhibit a softening curve, local softening instability can exist as a result of, say, the local buckling of stiffeners, lateral-torsional buckling due to inadequately provided torsional restraints and steel connections with semi-rigid joints.

A fruitful complementary analysis, especially for preliminary assessment or design, is to compute some bound to the maximum load that the structure can sustain. The use of so-called "direct" or "simplified" methods, which avoids a computationally expensive time-stepping analysis, represents a useful, competitive and increasingly appealing alternative. One important class of such methods is limit analysis. The distinctive feature of classical limit analysis is the determination of the load factor (or more precisely in practice, its upper and/or lower bounds) at which a critical event occurs, namely plastic collapse (see e.g. Massonnet and Save (1965); Kamenjarzh (1996); Carvelli, Maier, and Taliercio (2000); Leu and Chen (2006); Chen, Liu, and Cen (2008)).

The upper and lower bound theorems underpinning classical limit analysis are, however, strictly only applicable to structures that satisfy some rather restrictive (often onerous) requirements, the main ones being rigid perfect plasticity (no hardening or softening), geometric linearity and sufficiently large ductility. For instance, in the presence of softening, the pair of well-known bound theorems underpinning classical limit analysis is inapplicable. Also, local failure may well precede the plastic collapse of the structure predicted on the basis of unlimited ductility of

plastic hinges.

The clear practical need to overcome such shortcomings of classical limit analysis has motivated a number of research works, e.g. Ferris and Tin-Loi (2001); Tin-Loi, Tangaramvong, and Xia (2007); Ardito, Cocchetti, and Maier (2008). However, this is not a computationally easy task: the underlying mathematical programming problem that needs to be solved is a challenging one, often considered to be ill-posed in view of the numerical instabilities caused by lack of convexity and smoothness. The development of robust algorithmic approaches is thus essential.

The main purpose of this paper is to extend classical limit analysis to account for geometric and physical (softening) effects and limited ductility constraints. More explicitly, we consider the effects of combined axial and flexural force, local softening material behavior and 2nd-order nonlinear geometry, simultaneously, while at the same time satisfy some restrictions on ductility.

The present work was strongly motivated by Maier's proposal for a single-step simultaneous load and deformation analysis (see e.g. Ardito, Cocchetti, and Maier (2008) and listed references) and is a nontrivial extension of recent research [Tangaramvong and Tin-Loi (2009)] that considered 2nd-order geometric effects, albeit within a perfect plasticity context.

The term "limited ductility", it should be mentioned, is used in quite a general sense and encompasses limits on such quantities as plastic strains (including rotations), plastic work, total displacements at specific points of the structures, etc. As a result, the proposed method is able to compute in a single step an upper bound on the maximum load characterizing the proportionally applied loading. Deformations corresponding to that load will be automatically recovered at the same time.

The computational approach proposed is founded on the reasonable premise that the material behavior is holonomic or path-independent. This assumption, it is recalled, has been fully validated for the class of structures considered, see e.g. Tangaramvong and Tin-Loi (2007a). In fact, the holonomy assumption will often provide a close or even exact prediction of the actual structural response.

The extended limit analysis approach proposed is conceptually simple in that it aims to maximize the load factor (assumed to be a variable) under the same set of conditions that would apply to a holonomic analysis under load control. The difficulty lies in solving the resulting challenging optimization problem, referred to, in the mathematical programming literature [Luo, Pang, and Ralph (1996)], as a mathematical program with equilibrium constraints (MPEC). These equilibrium constraints are more precisely, in the present case, complementarity constraints and, in view of their nonconvexity and nonsmoothness, represent the main source of difficulty in solving MPECs.

The organization of the present paper is as follows. In Section 2, we describe the basic ingredients required for the appropriate formulations. These include discretization, Lagrangian description of statics and kinematics, and softening law. This is followed, in Section 3, by a review of the holonomic elastoplastic analysis of structures. An event-by-event holonomic algorithm is proposed to trace the overall structural response. Using the same set of governing holonomic relations, we develop, in Section 4, the required MPEC formulation for the extended limit analysis problem. In Section 5, we propose three nonlinear programming (NLP) based algorithms to solve the MPEC. Direct solution of the MPEC with the complementarity constraints described as $\mathbf{w}^{\mathrm{T}}\mathbf{z} = 0$, as done in Cocchetti and Maier (2003), will only work in some cases. Three numerical examples of practical, reasonably-sized structures are given in Section 6 to illustrate application of the proposed approach. Finally, some pertinent conclusions are drawn in Section 7.

A word regarding notation is in order. Vectors and matrices are indicated in bold. A real vector $\mathbf{x}$ of size m is indicated by $\mathbf{x} \in \Re^m$ and a real $m \times n$ matrix $\mathbf{A}$ by $\mathbf{A} \in \Re^{m\times n}$. For brevity, a vector of functions $\mathbf{f}(\mathbf{x}) : \Re^m \rightarrow \Re^n$ is written simply as $\mathbf{f} \in \Re^n$.

2 Preliminaries

2.1 Discrete structural model

A conventional lumped plasticity model within a "line" finite element framework, see e.g. DeDonato and Maier (1972); Bolzon and Corigliano (1997); Cocchetti and Maier (2003), is adopted in this study. This is appropriate since, for the frames under study, the plastic strains localize strongly in a limited number of fixed critical zones, whilst the remaining part of the structure can be considered to be still in the elastic regime.

The model for this kind of structural behavior then involves a special instance of the class of discrete formulations consisting of an elastic solid with embedded interfaces or loci of possible displacement discontinuities. These displacement discontinuities incorporate the localized dissipative effects observed in the failure of the material in the large-scale problem (e.g. a localized softening law between the bending moment and rotation), without the need to introduce explicitly the small scales [Ehrlich and Armero (2005); Armero and Ehrlich (2006)]. In fact, this generic representation [Bolzon and Corigliano (1997)] can be used to describe softening hinges as well as decohesion and quasibrittle fracture processes, through interface laws which relate tractions to displacement jumps.

An important implication of such finite element models is that mesh objectivity is ensured [Maier, Zavelani, and Dotreppe (1973)] even in the presence of local

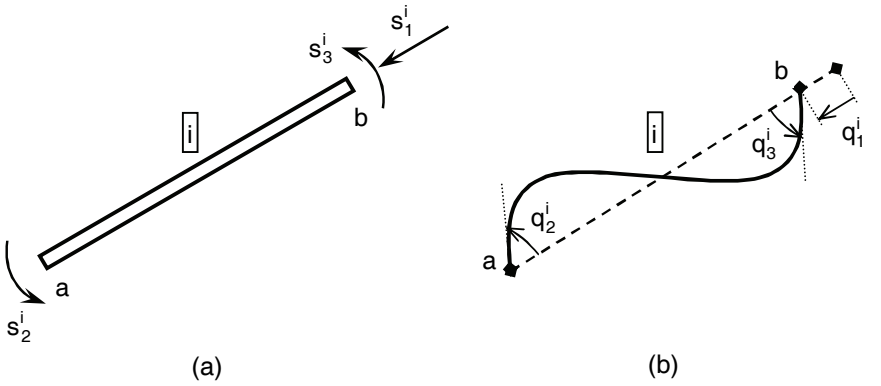

Figure 1: Generic 2-D frame element i (a) generalized stresses, (b) generalized strains.

softening behavior.

It is first assumed, as is usual, that the structure under consideration has been discretized as an aggregate of finite elements. In the present case, the material behavior is directly reflected by the element behavior, since the class of finite elements expressed in intrinsic, natural (in Prager's generalized sense) variables is adopted [Maier (1970)]. This implies that the scalar product of generalized stress and strain vectors represents virtual work in the element concerned and is invariant with respect to rigid body motion. In particular, the stress resultant or generalized stress is obtained by integrating the assumed stress field across the section. Similarly, the associated strain resultant is computed by a suitable kinematic assumption associating each physical component of strains with displacements in global coordinates.

To provide a better understanding, consider the generic self equilibrated 2-D frame element i shown in Fig. 1. For this element, the generalized stress vector $\mathbf{s}^i \in \Re^3$ contains the three (independent) two end moments (s_2^i, s_3^i) and one axial force (s_1^i). The corresponding generalized strain vector $\mathbf{q}^i \in \Re^3$ then consists of the corresponding end rotations (q_2^i, q_3^i) and axial deformation (q_1^i), which are explicitly taken as summation products of the generalized elastic strain vector $\mathbf{e}^i \in \Re^3$ and the generalized plastic strain vector $\mathbf{p}^i \in \Re^3$. The effect of shear force is ignored. Thus, it does not contribute to the internal work. Instead, the shear force is considered as a reaction, whilst its corresponding deformation is abandoned.

The external loads are proportionally applied at the model nodes only. For example, distributed loads are simplified as concentrated forces and lumped to act on nodes.

For elastoplastic members, material nonlinearity is included through the traditional

concept of the generalized plastic hinge model. More specifically, the formation of such a hinge is confined only to the member ends. Thus, the material between these ends remains purely elastic. Since the structure modeling is made on the basis of well-known "line" frame elements, supplemented by the possibility of lumped discrete plastic hinges forming at member ends, spreading of plasticity through the depth of a cross-section is thus precluded. However, the spread of plasticity along the member can be captured with suitably fine discretization in critical regions. The locations of possible hinges are a priori ascertained, for instance, under concentrated loads, at supports where yielding is likely to occur, etc. In the case of distributed loading, a finer discretization is carried out in those regions where hinges are likely to be formed, e.g. DeDonato and Maier (1972).

2.2 Lagrangian description of statics and kinematics

Two fundamental ingredients required to describe the structural behavior are equilibrium and compatibility. Equilibrium involves the relations between the nodal applied forces $\mathbf{F}^i \in \Re^6$ and the elemental stress resultants $\mathbf{s}^i$, whilst the compatibility condition relates the member deformations $\mathbf{q}^i$ to the nodal displacements $\mathbf{u}^i \in \Re^6$.

Consider the generic self-equilibrated discretized 2-D frame element i of Fig. 2, where l and θ define respectively the undeformed member length and the original inclined angle measured in an anticlockwise direction with respect to the horizontal axis.

In view of geometric nonlinearity considerations, the general compatibility relation is written as a nonlinear function of $\mathbf{u}^i$ as follows:

$$\mathbf{q}^i = \mathbf{q}^i(\mathbf{u}^i). \tag{1}$$

The corresponding equilibrium relation is expressed through the compatibility matrix $\mathbf{C}^i \in \Re^{3\times 6}$ by

$$\mathbf{F}^i = \mathbf{C}^{i\mathrm{T}}\mathbf{s}^i, \tag{2}$$

where

$$\mathbf{C}^i = \frac{\partial \mathbf{q}^i}{\partial \mathbf{u}^i}. \tag{3}$$

Clearly, the exact expressions for Eqs. 1-3 are nonlinear, and can be consistently approximated to any "order". In particular, an nth-order formulation is generated by retaining terms up to $(n-1)$th powers.

A simplified approach is based on the reasonable 2nd-order geometry approximation often used for slender structures, e.g. Maier (1971); Tin-Loi and Vimonsatit

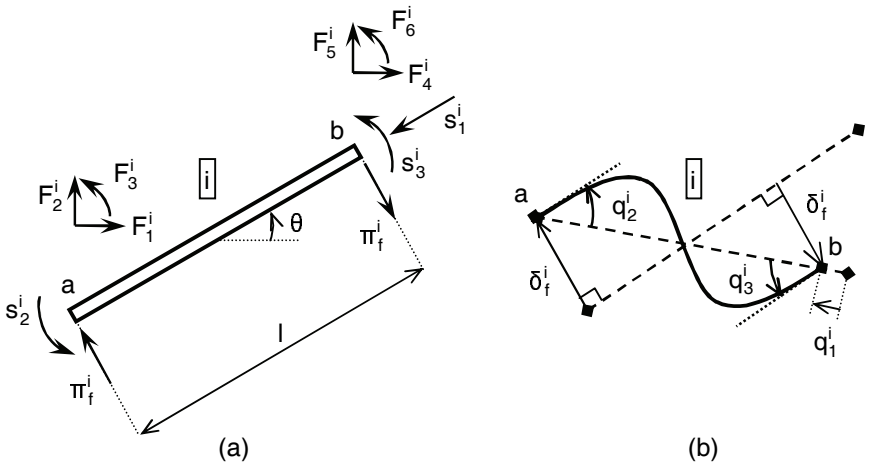

Figure 2: Generic 2-D frame element i with 2nd-order geometric nonlinearity (a) stresses, (b) strains.

(1996); Bolzon and Tin-Loi (1999), for which the 1st-power quantities of the exact geometrically nonlinear formulation are retained. It is then assumed that displacements from the undeformed state are geometrically small [Maier and Drucker (1973)]. This assumption is sufficiently accurate for the class of structures considered herein.

The equilibrium condition for each elastic member i in the deformed state is then established by using the so-called geometric stiffness matrix $\mathbf{K}_G^i \in \Re^{6\times 6}$ [Przemieniecki (1985)]. This matrix accounts for change of configuration with loading.

For the frame element i, this 2nd-order geometric nonlinearity can be conveniently described by introducing an additional transverse force π_f^i as well as its conjugate displacement δ_f^i, as shown in Fig. 2. Clearly, the force π_f^i and the displacement δ_f^i represent the configuration change of the member.

The equilibrium Eq. 2 of the element i can therefore be explicitly expressed as follows:

$$\mathbf{F}^i = \mathbf{C}_0^{i\mathrm{T}}\mathbf{s}^i + \mathbf{C}_f^{i\mathrm{T}}\pi_f^i, \tag{4}$$

where

$$\mathbf{F}^{i\mathrm{T}} = \left[\begin{array}{cccccc} F_1^i & F_2^i & F_3^i & F_4^i & F_5^i & F_6^i \end{array} \right],$$

$$\mathbf{C}_0^{i\mathrm{T}} = \left[\begin{array}{ccc} \cos\theta & -\sin\theta/l & -\sin\theta/l \\ \sin\theta & \cos\theta/l & \cos\theta/l \\ 0 & 1 & 0 \\ -\cos\theta & \sin\theta/l & \sin\theta/l \\ -\sin\theta & -\cos\theta/l & -\cos\theta/l \\ 0 & 0 & 1 \end{array} \right],$$

$$\mathbf{C}_f^i = \left[\begin{array}{cccccc} -\sin\theta & \cos\theta & 0 & \sin\theta & -\cos\theta & 0 \end{array} \right].$$

Obviously, $\mathbf{C}_0^i \in \Re^{3\times 6}$ is the conventional linear compatibility matrix and $\mathbf{C}_f^i \in \Re^{1\times 6}$ the associated auxiliary compatibility matrix, respectively. It is clear that Eq. 4 is described in the undeformed framework. Thus, the duality relationship between equilibrium and compatibility of the structural system is meaningfully preserved. Moreover, since 2nd-order theory assumes small deformations, the compatibility Eq. 1 can be simply given by the following linear function:

$$\mathbf{q}^i = \mathbf{C}_0^i \mathbf{u}^i, \tag{5}$$

provided that an additional displacement δ_f^i, linearly proportional to nodal displacements $\mathbf{u}^i$, is introduced as follows:

$$\delta_f^i = \mathbf{C}_f^i \mathbf{u}^i. \tag{6}$$

It is further assumed that the structure considered is controlled solely by a monotonically increasing (or decreasing) single load multiplier α. Hence, the external nodal forces $\mathbf{F}^i$ are defined by

$$\mathbf{F}^i = \alpha \mathbf{f}^i + \mathbf{f}_d^i, \tag{7}$$

where $\mathbf{f}^i \in \Re^6$ and $\mathbf{f}_d^i \in \Re^6$ are the given basic nodal load vector controlled through α and the fixed nodal load vector, respectively.

By collecting Eqs. 4-7, the governing Lagrangian static-kinematic description at an element level becomes

$$\left[\begin{array}{ccc} \cdot & \mathbf{C}_0^{i\mathrm{T}} & \mathbf{C}_f^{i\mathrm{T}} \\ \mathbf{C}_0^i & \cdot & \cdot \\ \mathbf{C}_f^i & \cdot & \cdot \end{array} \right] \left[\begin{array}{c} \mathbf{u}^i \\ \mathbf{s}^i \\ \pi_f^i \end{array} \right] = \left[\begin{array}{c} \alpha \mathbf{f}^i + \mathbf{f}_d^i \\ \mathbf{q}^i \\ \delta_f^i \end{array} \right], \tag{8}$$

where symbol $(\cdot)$ represents a null vector or zero matrix of appropriate size.

For the entire structural system that has been discretized into n generic elements, d degrees of freedom and m natural generalized stresses (or strains), the equilibrium and compatibility conditions are

$$\begin{bmatrix} \cdot & \mathbf{C}_0^{\mathrm{T}} & \mathbf{C}_f^{\mathrm{T}} \\ \mathbf{C}_0 & \cdot & \cdot \\ \mathbf{C}_f & \cdot & \cdot \end{bmatrix} \begin{bmatrix} \mathbf{u} \\ \mathbf{s} \\ \pi_f \end{bmatrix} = \begin{bmatrix} \alpha\mathbf{f}+\mathbf{f}_d \\ \mathbf{q} \\ \delta_f \end{bmatrix}. \tag{9}$$

Self-evident indexless matrices $\mathbf{C}_0 \in \Re^{m\times d}$, $\mathbf{C}_f \in \Re^{n\times d}$ and vectors $\mathbf{f} \in \Re^d$, $\mathbf{f}_d \in \Re^d$, $\mathbf{u} \in \Re^d$ are assembled by using appropriate location vectors. The concatenated vectors $\mathbf{s} \in \Re^m$ and $\mathbf{q} \in \Re^m$ collect respectively all their corresponding elemental vectors, e.g. $\mathbf{s}^{\mathrm{T}} \equiv \left[\mathbf{s}^{1\mathrm{T}} \cdots \mathbf{s}^{n\mathrm{T}}\right]$ and $\mathbf{q}^{\mathrm{T}} \equiv \left[\mathbf{q}^{1\mathrm{T}} \cdots \mathbf{q}^{n\mathrm{T}}\right]$. Vectors $\pi_f \in \Re^n$ and $\delta_f \in \Re^n$ collect their n corresponding variables, e.g. $\pi_f^{\mathrm{T}} = \left[\pi_f^1, \ldots, \pi_f^n\right]$ and $\delta_f^{\mathrm{T}} = \left[\delta_f^1, \ldots, \delta_f^n\right]$, respectively.

2.3 Constitutive model

The key relations governing a complete specification of the constitutive behavior of a generic element, leading to that of the entire structure, are now briefly presented. In essence, these include strain decomposition, elasticity and plasticity. Furthermore, both 2nd-order geometric and nontraditional (softening) material nonlinearities are considered. The focus is on frame elements for which combined bending and axial force can affect yielding.

2.3.1 Strain decomposition

As clearly shown in Fig. 3, the additivity of member elastic and plastic strains is written as follows:

$$\mathbf{q}^i = \mathbf{e}^i + \mathbf{p}^i, \tag{10}$$

and, for the entire structural system, as

$$\mathbf{q} = \mathbf{e} + \mathbf{p}, \tag{11}$$

where $\mathbf{e}^{\mathrm{T}} \equiv \left[\mathbf{e}^{1\mathrm{T}} \cdots \mathbf{e}^{n\mathrm{T}}\right]$ and $\mathbf{p}^{\mathrm{T}} \equiv \left[\mathbf{p}^{1\mathrm{T}} \cdots \mathbf{p}^{n\mathrm{T}}\right]$.

2.3.2 Elasticity

When a 2nd-order approximation is considered to be sufficiently accurate, the well-known nodal geometric stiffness matrix $\mathbf{K}_G^i$ [Przemieniecki (1985)], as mentioned earlier, can be used. This, in particular, is generated by retaining terms up to and

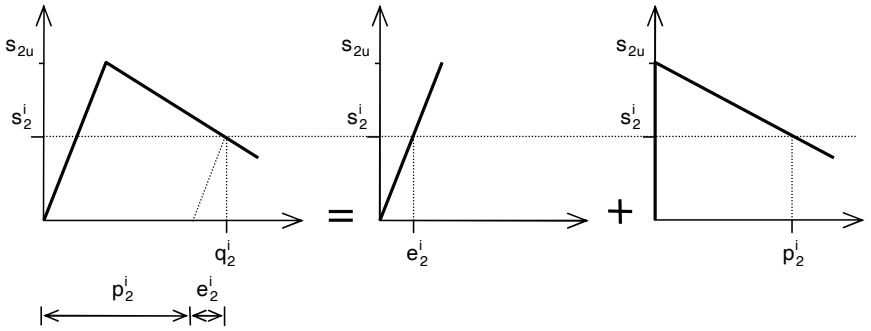

Figure 3: Generalized strain description.

including the 1st-power quantities of the exact formation, see e.g. DeFreitas and LloydSmith (1984–85); Tin-Loi and Vimonsatit (1996).

The elastic stiffness formulation (in Fig. 2) then consists of two components, namely the relation between stresses $\mathbf{s}^i$ and elastic strains $\mathbf{e}^i$ as well as that between an additional force π_f^i and its corresponding deformation δ_f^i.

Firstly, the appropriate stiffness relation between $\mathbf{s}^i$ and $\mathbf{e}^i$ is

$$\mathbf{s}^i = \left(\mathbf{S}_0^i + \mathbf{S}_g^i\right)\mathbf{e}^i, \tag{12}$$

where

$$\mathbf{S}_0^i = \begin{bmatrix} EA/l & 0 & 0 \\ 0 & 4EI/l & 2EI/l \\ 0 & 2EI/l & 4EI/l \end{bmatrix},$$

$$\mathbf{S}_g^i = \left(\frac{-s_1^i}{l}\right) \begin{bmatrix} 0 & 0 & 0 \\ 0 & 2l^2/15 & -l^2/30 \\ 0 & -l^2/30 & 2l^2/15 \end{bmatrix}.$$

It is noted that $\mathbf{S}_0^i \in \Re^{3\times 3}$ is a conventional (symmetric and positive definite) elastic stiffness matrix in the small deformation regime, and $\mathbf{S}_g^i \in \Re^{3\times 3}$ is an elemental geometric stiffness matrix accounting for 2nd-order effects, symmetric but not necessarily positive semidefinite. The total stiffness matrix $\mathbf{S}^i = \mathbf{S}_0^i + \mathbf{S}_g^i$. Eq. 12 clearly reduces to

$$\mathbf{s}^i = \mathbf{S}^i\mathbf{e}^i. \tag{13}$$

Secondly, the relation between π_f^i and δ_f^i is

$$\pi_f^i = S_f^i\delta_f^i, \tag{14}$$

where

$$S_f^i = \left(-\frac{s_1^i}{l}\right).$$

It is useful to compare our 2nd-order formulation with the nodal force-displacement relation of Przemieniecki (1985). By assuming $\theta = 0$, and collecting Eqs. 8, 12 and 14 yields the following relationship between the nodal forces $\mathbf{F}^i$ and the displacements $\mathbf{u}^i$ of an elastic member i:

$$\mathbf{F}^i = \left(\mathbf{C}_0^{i\mathrm{T}}\mathbf{S}_0^i\mathbf{C}_0^i\right)\mathbf{u}^i + \left(\mathbf{C}_0^{i\mathrm{T}}\mathbf{S}_g^i\mathbf{C}_0^i + \mathbf{C}_f^{i\mathrm{T}}S_f^i\mathbf{C}_f^i\right)\mathbf{u}^i, \tag{15}$$

where

$$\mathbf{C}_0^{i\mathrm{T}}\mathbf{S}_0^i\mathbf{C}_0^i = \frac{EI}{l^3}\begin{bmatrix} Al^2/I & 0 & 0 & -Al^2/I & 0 & 0 \\ 0 & 12 & 6l & 0 & -12 & 6l \\ 0 & 6l & 4l^2 & 0 & -6l & 2l^2 \\ -Al^2/I & 0 & 0 & Al^2/I & 0 & 0 \\ 0 & -12 & -6l & 0 & 12 & -6l \\ 0 & 6l & 2l^2 & 0 & -6l & 4l^2 \end{bmatrix},$$

$$\mathbf{C}_0^{i\mathrm{T}}\mathbf{S}_g^i\mathbf{C}_0^i + \mathbf{C}_f^{i\mathrm{T}}S_f^i\mathbf{C}_f^i = -\frac{s_1^i}{l}\begin{bmatrix} 0 & 0 & 0 & 0 & 0 & 0 \\ 0 & 6/5 & l/10 & 0 & -6/5 & l/10 \\ 0 & l/10 & 2l^2/15 & 0 & -l/10 & -l^2/30 \\ 0 & 0 & 0 & 0 & 0 & 0 \\ 0 & -6/5 & -l/10 & 0 & 6/5 & -l/10 \\ 0 & l/10 & -l^2/30 & 0 & -l/10 & 2l^215 \end{bmatrix}.$$

Clearly, Eq. 15 coincides with the nodal force-displacement equation of Przemieniecki (1985), provided that the nodal elastic stiffness matrix $\mathbf{K}_0^i \in \Re^{6\times 6}$ and the nodal geometrical stiffness matrix $\mathbf{K}_G^i \in \Re^{6\times 6}$ are respectively

$$\mathbf{K}_0^i = \mathbf{C}_0^{i\mathrm{T}}\mathbf{S}_0^i\mathbf{C}_0^i, \tag{16}$$

$$\mathbf{K}_G^i = \mathbf{C}_0^{i\mathrm{T}}\mathbf{S}_g^i\mathbf{C}_0^i + \mathbf{C}_f^{i\mathrm{T}}S_f^i\mathbf{C}_f^i. \tag{17}$$

Hence, Eq. 15 can be rewritten as follows:

$$\mathbf{F}^i = \mathbf{K}_0^i\mathbf{u}^i + \mathbf{K}_G^i\mathbf{u}^i. \tag{18}$$

It should be noted that both $\mathbf{S}_g^i$ in Eq. 12 and S_f^i in Eq. 14 depend on the single axial force s_1^i. Thus, a zero axial force ($s_1^i = 0$) implies geometric linearity, which simply indicates $\mathbf{S}^i = \mathbf{S}_0^i$.

For the entire structural system, the elastic stiffness given by Eqs. 13-14 for all n elements are assembled from

$$\mathbf{s} = \mathbf{S}\mathbf{e}, \tag{19}$$

$$\pi_f = \mathbf{S}_f \delta_f, \tag{20}$$

where

$$\mathbf{S} = \mathbf{S}_0 + \mathbf{S}_g, \tag{21}$$

$\mathbf{S} \in \Re^{m\times m}$, $\mathbf{S}_0 \in \Re^{m\times m}$, $\mathbf{S}_g \in \Re^{m\times m}$ and $\mathbf{S}_f \in \Re^{n\times n}$.

2.3.3 Softening

As indicated in the foregoing, the material behavior considered in this paper falls in the category of elastoplastic softening constitutive laws. The focus of this subsection is on a mathematical description of the so-called holonomic (or path-independent) plasticity model.

When, as in beams, it is accurate enough to represent the plastic hinge solely by a moment-rotation relationship (as in Fig. 3), the softening laws proposed by Tin-Loi and Xia (2001) can be used. However, when members (e.g. heavily loaded columns) are subjected to significant combined axial and flexural forces, the effects of axial forces on the yield condition must be included. The mathematical description as to how this is achieved is provided in the following.

In the first instance, the computationally advantageous piecewise linear approximation to a nonlinear yield surface has been adopted. In essence, a priori piecewise linearization of the nonlinear yield hypersurface is assumed, as popularized by Maier and his group, e.g. Maier (1970); Maier (1971); DeDonato and Maier (1972).

Without undue loss of generality, the present description refers specifically to the commonly used hexagonal piecewise linear yield locus shown in Fig. 4 for the "start" hinge a of an element i. This yield locus is typical of an I-steel section under combined bending and axial force [Massonnet and Save (1965)], where γ is the angle defining the orientation of the inclined yield hyperplanes. It is also assumed that positive and negative flexural/axial properties are identical, and that a reduction of the pure bending capacity occurs when the axial force reaches some fraction (specified through the factor r_b, normally set to 0.15) of the pure axial capacity.

In a similar manner to Cocchetti, Maier, and Shen (2002), when the material is subject to the softening (or hardening) behavior the adopted constitutive law describes

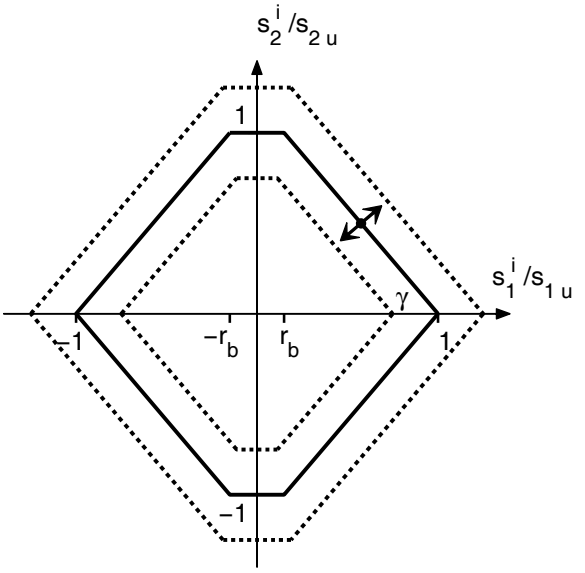

Figure 4: Hexagonal piecewise linear yield locus.

the evolution of isotropic softening (or hardening) yield surfaces. More specifically, as shown by the inner dashed lines in Fig 4, the isotropic softening model defines a uniformly shrinking yield locus without shape changes. In the same way, the isotropic hardening model indicates a homothetically expanding of the yield surface (i.e. outer dashed lines in Fig. 4).

The particular assumption of isotropic softening and hardening, it is worth mentioning, is not important for realistic structures under monotonically applied loads since it is unlikely that progressive softening or hardening will activate the opposite yield plane.

As mentioned earlier, the intrinsic material behavior is based on the holonomic or path-independent elastoplastic assumption. Holonomy, in the spirit of the deformation theory of plasticity, implies that elastic unloading does not occur and that the stress point (as indicated by the arrows in Fig. 5) is restricted to move along the actual branches. Thus, any unloading from the active yield branch is reversible in nature.

As indicated in Tangaramvong and Tin-Loi (2007a), a holonomic, rather than the less tractable nonholonomic, analysis is sufficiently accurate in the prediction of the response of such structures under monotonically applied loads. This is due to

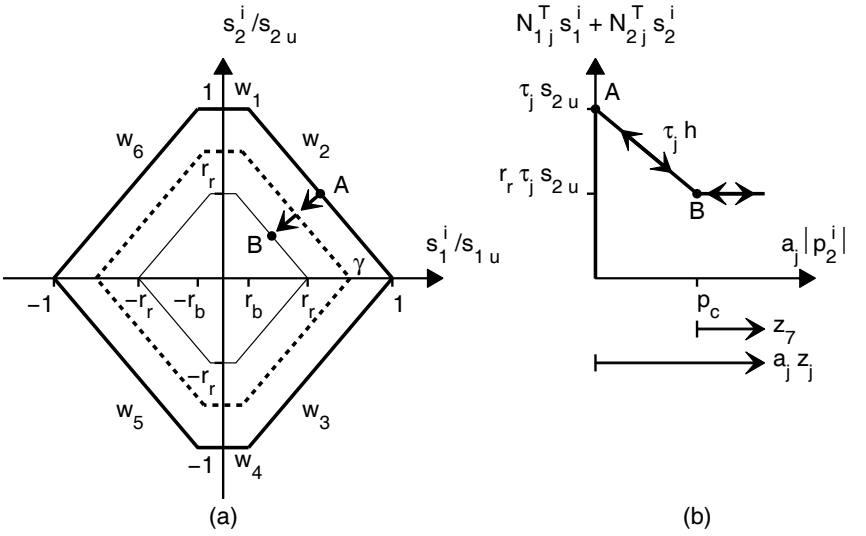

Figure 5: Piecewise linear softening law (a) interaction between bending and axial forces, (b) typical holonomic behavior for yield plane j.

the fact that the overall structural behavior is largely unaffected by the occurrence of nonholonomic unloading.

Underpinning the description of the holonomic law is the well-known mathematical structure known as "complementarity". The complementarity conditions imply, for total quantities, the componentwise relationship $w_j \geq 0, z_j \geq 0, w_j z_j = 0$ for all j. For vectors $\mathbf{w}^a \geq \mathbf{0}$ and $\mathbf{z}^a \geq \mathbf{0}$, this condition is typically written as $\mathbf{w}^{a\mathrm{T}}\mathbf{z}^a = 0$. Mechanically, with w_j representing a yield function and z_j a plastic multiplier, it implies that plastic yielding $(w_j = 0)$ can only occur if the stress point is actually on the yield surface $(z_j > 0)$, and hence $w_j z_j = 0$. Moreover, if the material is still elastic $(w_j > 0)$ then there is no plastic flow $(z_j = 0)$, again satisfying the complementarity condition $w_j z_j = 0$.

With reference to the hexagonal yield surface in Fig. 5, the dimensionless s_2^i/s_{2u} versus s_1^i/s_{1u} graph is used to represent the isotropic softening interaction between axial force s_1^i and bending moment s_2^i of a hinge a, where s_{1u} and s_{2u} are respectively their corresponding yield capacities. The homothetic shrinking (dashed lines) of the yield domain is assumed to cease at the residual state r_r (thin line).

The holonomic constitutive law describing this model is then as follows:

$$\mathbf{w}^a = -\mathbf{N}^{a\mathrm{T}}\mathbf{s}^a + \mathbf{H}^a\mathbf{z}^a + \mathbf{r}^a \geq \mathbf{0}, \mathbf{z}^a \geq \mathbf{0}, \mathbf{w}^{a\mathrm{T}}\mathbf{z}^a = 0, \tag{22}$$

where

$$\mathbf{w}^{a\mathrm{T}} = \begin{bmatrix} w_1 & w_2 & w_3 & w_4 & w_5 & w_6 & w_7 \end{bmatrix},$$

$$\mathbf{s}^{a\mathrm{T}} = \begin{bmatrix} s_1^i & s_2^i \end{bmatrix},$$

$$\mathbf{z}^{a\mathrm{T}} = \begin{bmatrix} z_1 & z_2 & z_3 & z_4 & z_5 & z_6 & z_7 \end{bmatrix},$$

$$\mathbf{N}^a = \begin{bmatrix} 0 & \widehat{n} & \widehat{n} & 0 & -\widehat{n} & -\widehat{n} & 0 \\ 1 & 1 & -1 & -1 & -1 & 1 & 0 \end{bmatrix},$$

$$\mathbf{H}^a = h \begin{bmatrix} a_1 & a_2 & a_3 & a_4 & a_5 & a_6 & -1 \\ \tau a_1 & \tau a_2 & \tau a_3 & \tau a_4 & \tau a_5 & \tau a_6 & -\tau \\ \tau a_1 & \tau a_2 & \tau a_3 & \tau a_4 & \tau a_5 & \tau a_6 & -\tau \\ a_1 & a_2 & a_3 & a_4 & a_5 & a_6 & -1 \\ \tau a_1 & \tau a_2 & \tau a_3 & \tau a_4 & \tau a_5 & \tau a_6 & -\tau \\ \tau a_1 & \tau a_2 & \tau a_3 & \tau a_4 & \tau a_5 & \tau a_6 & -\tau \\ a_1 & a_2 & a_3 & a_4 & a_5 & a_6 & -1 \end{bmatrix},$$

$$\mathbf{r}^{a\mathrm{T}} = \begin{bmatrix} s_{2u} & \tau s_{2u} & \tau s_{2u} & s_{2u} & \tau s_{2u} & \tau s_{2u} & s_{2u}(1-r_r) \end{bmatrix},$$

$\widehat{n} = (s_{2u}/s_{1u}) \tan\gamma$, $h = -s_{2u}(1-r_r)/p_c$, $\tau = 1 + r_b \tan\gamma$, and $a_j = p_c / \left|p_{cj}\right|$ for all $j \in \{1,\ldots,6\}$. It is obvious that the softening matrix $\mathbf{H}^a$ is nonsymmetric.

For clarity, the softening behavior of a typical yield hyperplane $j \in \{1,\ldots,6\}$ is plotted on the combined stresses $(N_{1j}^{\mathrm{T}} s_1^i + N_{2j}^{\mathrm{T}} s_2^i)$ versus scaled plastic strain $a_j \left|p_2^i\right|$ space in Fig. 5; N_{1j} and N_{2j} are normals projected respectively on the s_1^i and s_2^i axes; a_j defines a scaling factor applied to the plastic multiplier z_j. As is usual for the hexagonal yield shape, the scalars $\tau_j\,(j = 2,3,5,6) = \tau$, and $\tau_j\,(j = 1,4) = 1$. For convenience, the breakpoint between the softening and flat portions for each hyperplane j is defined by a single, arbitrarily assumed critical plastic strain p_c (e.g. $p_c = p_{c1}$), in which $p_{cj}\,(j = 1,\ldots,6)$ are the actual critical plastic strain values.

The yield functions w_1 to w_6 essentially describe a softening evolution of their corresponding yield hyperplanes 1 to 6, as shown by the dashed lines in Fig. 5. An additional yield function w_7 is required to express the movement of a yield point on the horizontal (residual) portion, as per the thin line in the hexagonal diagram. This evolution, for instance, is illustrated by the stress point moving along AB, as indicated in this figure. Physically, the elastic boundary is first reached at point A on the activated hyperplane, and then the material softens isotropically. Since an isotropic softening model is assumed, the other hyperplanes also simultaneously shrink, with the result that the original hexagonal yield polygon becomes smaller but still retains its shape. The stress point thus moves on the inclined softening branch until it reaches the breakpoint B (corresponding to the smallest yield polygon in Fig. 5), after which it moves along the horizontal (perfectly plastic) branch.

These complementarity conditions, it should be noted, need to predict precisely the various cases when no solution or multiple solutions arise. For example, for the piecewise linear softening representation shown in Fig. 5, when $r_r\tau_j s_{2u} < N_{1j}^{\mathrm{T}} s_1^i + N_{2j}^{\mathrm{T}} s_2^i < \tau_j s_{2u}$ the complementarity model should be able to recover precisely two solutions for $a_j \left| p_2^i \right|$ (i.e. one with $a_j \left| p_2^i \right| = 0$ on the vertical elastic branch and the other with $a_j \left| p_2^i \right| > 0$ on the inclined softening branch). Additionally, for any given $0 < a_j \left| p_2^i \right| < p_c$, the expression for the softening law should furnish, as is clear, a unique solution for $N_{1j}^{\mathrm{T}} s_1^i + N_{2j}^{\mathrm{T}} s_2^i$. However, when $N_{1j}^{\mathrm{T}} s_1^i + N_{2j}^{\mathrm{T}} s_2^i > \tau_j s_{2u}$, there exists no solution for any $a_j \left| p_2^i \right|$.

The softening constitutive relations for a typical frame element i are generated by assembling the corresponding relations for the two end hinges a and b. For simplicity, it is assumed that the inelastic properties of these hinges a and b are identical, which means that a similar set of functions as in Eq. 22 can be collected for node b, e.g. $\mathbf{H}^a = \mathbf{H}^b$ and $\mathbf{r}^a = \mathbf{r}^b$. The softening laws at an element level can then be written as follows:

$$\mathbf{w}^i = -\mathbf{N}^{i\mathrm{T}} \mathbf{s}^i + \mathbf{H}^i \mathbf{z}^i + \mathbf{r}^i \geq \mathbf{0}, \mathbf{z}^i \geq \mathbf{0}, \mathbf{w}^{i\mathrm{T}} \mathbf{z}^i = 0, \tag{23}$$

where

$$\mathbf{w}^{i\mathrm{T}} = \begin{bmatrix} \mathbf{w}^{a\mathrm{T}} & \mathbf{w}^{b\mathrm{T}} \end{bmatrix}, \mathbf{s}^{i\mathrm{T}} = \begin{bmatrix} s_1^i & s_2^i & s_3^i \end{bmatrix},$$
$$\mathbf{z}^{i\mathrm{T}} = \begin{bmatrix} \mathbf{z}^{a\mathrm{T}} & \mathbf{z}^{b\mathrm{T}} \end{bmatrix}, \mathbf{r}^{i\mathrm{T}} = \begin{bmatrix} \mathbf{r}^{a\mathrm{T}} & \mathbf{r}^{b\mathrm{T}} \end{bmatrix},$$

$$\mathbf{N}^i = \begin{bmatrix} 0 & \widehat{n} & \widehat{n} & 0 & -\widehat{n} & -\widehat{n} & 0 & 0 & \widehat{n} & \widehat{n} & 0 & -\widehat{n} & -\widehat{n} & 0 \\ 1 & 1 & -1 & -1 & -1 & 1 & 0 & 0 & 0 & 0 & 0 & 0 & 0 & 0 \\ 0 & 0 & 0 & 0 & 0 & 0 & 0 & 1 & 1 & -1 & -1 & -1 & 1 & 0 \end{bmatrix},$$

$$\mathbf{H}^i = \begin{bmatrix} \mathbf{H}^a & \cdot \\ \cdot & \mathbf{H}^b \end{bmatrix}.$$

Finally, the holonomic constitutive relations for the entire discrete structure, made up of n elements and y yield functions, can be suitably assembled as in conventional finite element formalism as follows:

$$\mathbf{w} = -\mathbf{N}^{\mathrm{T}} \mathbf{s} + \mathbf{H}\mathbf{z} + \mathbf{r} \geq \mathbf{0}, \mathbf{z} \geq \mathbf{0}, \mathbf{w}^{\mathrm{T}} \mathbf{z} = 0. \tag{24}$$

Obviously, the new and self-evident indexless symbols collect all $i \in \{1, \ldots, n\}$ element vectors and matrices as concatenated vectors and block-diagonal matrices, respectively. For instance, $\mathbf{w}^{\mathrm{T}} \in \Re^y \equiv \left[\mathbf{w}^{1\mathrm{T}} \cdots \mathbf{w}^{n\mathrm{T}}\right]$, $\mathbf{z}^{\mathrm{T}} \in \Re^y \equiv \left[\mathbf{z}^{1\mathrm{T}} \cdots \mathbf{z}^{n\mathrm{T}}\right]$, $\mathbf{r}^{\mathrm{T}} \in \Re^y \equiv \left[\mathbf{r}^{1\mathrm{T}} \cdots \mathbf{r}^{n\mathrm{T}}\right]$, $\mathbf{N} \in \Re^{m \times y} \equiv diag\left(\mathbf{N}^1, \ldots, \mathbf{N}^n\right)$, and $\mathbf{H} \in \Re^{y \times y} \equiv diag\left(\mathbf{H}^1, \ldots, \mathbf{H}^n\right)$.

The plastic deformation vector $\mathbf{p}$ for the entire structure, it is worth mentioning, is defined through the associated flow rule. More explicitly, this expresses the fact that

the plastic strains $\mathbf{p}$ are functions of the plastic multipliers $\mathbf{z}$ through the constant matrix of outward normals $\mathbf{N}$, as in the following:

$$\mathbf{p} = \mathbf{N}\mathbf{z}. \tag{25}$$

3 Holonomic elastoplastic analysis

In this section, the prescribed three basic ingredients, namely statics, kinematics and constitution, are collected to formulate the holonomic state problem. These form the basis for the analysis of the considered structure accounting for both material (softening) and 2nd-order geometric nonlinearities simultaneously.

The governing holonomic Eqs. 9, 11, 19, 20, 24 and 25 can be simplified by retaining variables $(\mathbf{s}, \pi_f, \mathbf{u}, \mathbf{z})$ as follows:

$$\begin{bmatrix} \cdot & \mathbf{C}_0^{\mathrm{T}} & \mathbf{C}_f^{\mathrm{T}} & \cdot \\ -\mathbf{C}_0 & \mathbf{S}^{-1} & \cdot & \mathbf{N} \\ -\mathbf{C}_f & \cdot & \mathbf{S}_f^{-1} & \cdot \\ \cdot & -\mathbf{N}^{\mathrm{T}} & \cdot & \mathbf{H} \end{bmatrix} \begin{bmatrix} \mathbf{u} \\ \mathbf{s} \\ \pi_f \\ \mathbf{z} \end{bmatrix} = \begin{bmatrix} \cdot \\ \cdot \\ \cdot \\ \mathbf{w} \end{bmatrix} + \begin{bmatrix} \alpha\mathbf{f} + \mathbf{f}_d \\ \cdot \\ \cdot \\ -\mathbf{r} \end{bmatrix},$$

$$\mathbf{w} \geq \mathbf{0},\ \mathbf{z} \geq \mathbf{0},\ \mathbf{w}^{\mathrm{T}}\mathbf{z} = 0. \tag{26}$$

It should be noted that Eq. 26 constitutes an instance of the class of mathematical programs known as a mixed complementarity problem (MCP) [Dirkse and Ferris (1995)].

The MCP in effect represents the Karush-Kuhn-Tucker (KKT) conditions of typically some extremum principle. It is often computationally advantageous to solve this MCP rather than an optimization problem, e.g. Maier (1970); Liu and Atluri (2008).

A key advantage of using the fictitious forces π_f is now apparent in that it leads to a standard MCP (nonsymmetric) form [Cottle, Pang, and Stone (1992)]. Not only does this allow theoretical results, such as those concerning existence and uniqueness, to be obtained, but it also presents a numerically more stable mathematical structure to process, for instance by any one of available state-of-the art solvers, such as GAMS/PATH [Dirkse and Ferris (1995)] which can be called, as in our work, from within the powerful GAMS mathematical programming modeling environment. GAMS is an acronym for General Algebraic Modeling System [Brooke, Kendick, Meeraus, and Raman (1998)].

A traditional holonomic analysis is typically performed in a single-step fashion. For a given load α, the complete response of the structure for that state is simply computed, and the multiple equilibrium branches (if they exist) can be captured

by using, for instance, special enumerative algorithms [Tin-Loi and Tseng (2003); Tin-Loi, Tangaramvong, and Xia (2007)]. Thus, the whole spectrum of structural responses in a prescribed load regime can be mapped out through a series of single-step MCP solves.

Even though it is conceptually simpler, this direct holonomic approach may not be the most efficient computational approach. This is due to the fact that all yield functions are simultaneously processed, thus leading to typically large problem sizes.

Our algorithm attempts to solve the holonomic problem in a similar fashion to a nonholonomic analysis. This approach traces event-by-event the holonomic structural responses so that all yield activations can be identified. In essence, the method used follows the nonholonomic algorithm proposed in our recent work [Tangaramvong and Tin-Loi (2007a)] for the small deflection case.

Instead of using Eq. 26, we retain only variables $\mathbf{z}$ leading to the following more compact form that in effect is a linear complementarity problem (LCP) [Cottle, Pang, and Stone (1992)]:

$$\begin{aligned} \mathbf{w} &= -\mathbf{N}^{\mathrm{T}}\mathbf{S}\mathbf{C}_0\mathbf{K}^{-1}\left(\alpha\mathbf{f}+\mathbf{f}_d\right)+\left(\mathbf{H}-\mathbf{N}^{\mathrm{T}}\mathbf{Z}\mathbf{N}\right)\mathbf{z}+\mathbf{r}, \\ &\mathbf{w}\geq\mathbf{0},\ \mathbf{z}\geq\mathbf{0},\ \mathbf{w}^{\mathrm{T}}\mathbf{z}=0, \end{aligned} \tag{27}$$

where

$$\mathbf{Z}=\mathbf{S}\mathbf{C}_0\mathbf{K}^{-1}\mathbf{C}_0^{\mathrm{T}}\mathbf{S}-\mathbf{S}, \tag{28}$$

$$\mathbf{K}=\mathbf{K}_0+\mathbf{K}_G, \tag{29}$$

$$\mathbf{K}_0=\mathbf{C}_0^{\mathrm{T}}\mathbf{S}_0\mathbf{C}_0, \tag{30}$$

$$\mathbf{K}_G=\mathbf{C}_0^{\mathrm{T}}\mathbf{S}_g\mathbf{C}_0+\mathbf{C}_f^{\mathrm{T}}\mathbf{S}_f\mathbf{C}_f. \tag{31}$$

Matrix $\mathbf{K}_G$ is the well-known symmetric geometric stiffness of the assembled structure [Przemieniecki (1985)].

The algorithm adopted is outlined as follows. The aim is to calculate the configuration change $\Delta\Sigma$ involving such variables as $\Delta\mathbf{s},\Delta\mathbf{u},\Delta\mathbf{z},\Delta\mathbf{w}$ from the previous known state $\overline{\Sigma}$ described by quantities such as $\overline{\alpha},\overline{\mathbf{s}},\overline{\mathbf{u}},\overline{\mathbf{z}},\overline{\mathbf{w}}$ so that the current unknown state $\Sigma=\overline{\Sigma}+\Delta\Sigma$ can be found. Clearly,

$$\begin{aligned} \alpha &= \bar{\alpha}+\Delta\alpha, \\ \mathbf{s} &= \bar{\mathbf{s}}+\Delta\mathbf{s}, \\ \mathbf{u} &= \bar{\mathbf{u}}+\Delta\mathbf{u}, \\ \mathbf{z} &= \bar{\mathbf{z}}+\Delta\mathbf{z}, \\ \mathbf{w} &= \bar{\mathbf{w}}+\Delta\mathbf{w}, \end{aligned} \tag{32}$$

where the incremental step $\Delta\alpha$ is varied to capture exactly critical events, such as activation of a new yield plane. By substituting Eq. 32 into Eq. 27, the following standard LCP can be obtained:

$$\mathbf{w} = \mathbf{A}\Delta\mathbf{z} - \mathbf{b}\Delta\alpha + \mathbf{c} \geq \mathbf{0}, \mathbf{z} \geq \mathbf{0}, \mathbf{w}^{\mathrm{T}}\mathbf{z} = 0, \tag{33}$$

where

$$\begin{aligned} &\mathbf{A} = \mathbf{H} - \mathbf{N}^{\mathrm{T}}\mathbf{Z}\mathbf{N}, \\ &\mathbf{b} = \mathbf{N}^{\mathrm{T}}\mathbf{S}\mathbf{C}_0\mathbf{K}^{-1}\mathbf{f}, \\ &\mathbf{c} = (\mathbf{H} - \mathbf{N}^{\mathrm{T}}\mathbf{Z}\mathbf{N})\bar{\mathbf{z}} - \mathbf{N}^{\mathrm{T}}\mathbf{S}\mathbf{C}_0\mathbf{K}^{-1}(\overline{\alpha}\mathbf{f} + \mathbf{f}_d) + \mathbf{r}. \end{aligned} \tag{34}$$

In the state $\overline{\Sigma}$, it is straightforward to set up an active set $\{t\}$ (for which $\overline{\mathbf{w}} = \mathbf{0}$) and a nonactive set $\{p\}$ (for which $\overline{\mathbf{w}} > \mathbf{0}$). The set $\{t\}$ is further partitioned into two subsets, namely the active set $\{a\}$ having no plastic multipliers ($\bar{\mathbf{z}}_t = \mathbf{0}$) and the active set $\{b\}$ containing some plastic multipliers ($\bar{\mathbf{z}}_t > \mathbf{0}$). These two subsets allow for reversal of plastic multipliers at the same time as prohibiting any elastic stress unloading. Eq. 33 is then rearranged with respect to these three sets $\{a\}$, $\{b\}$ and $\{p\}$. During a step $\Delta\alpha$, the nonactive set $\{p\}$ is assumed to remain constant (i.e. $\mathbf{w}_p \geq \mathbf{0}$ and $\mathbf{z}_p = \mathbf{0}$), and only the active sets $\{a\}$ and $\{b\}$ are considered. Hence, this leads to the following MCP:

$$\begin{aligned} &\mathbf{w}_b = \mathbf{A}_{bb}\Delta\mathbf{z}_b + \mathbf{A}_{ba}\Delta\mathbf{z}_a - \mathbf{b}_b\Delta\alpha + \mathbf{c}_b = \mathbf{0}, \\ &\mathbf{w}_a = \mathbf{A}_{ab}\Delta\mathbf{z}_b + \mathbf{A}_{aa}\Delta\mathbf{z}_a - \mathbf{b}_a\Delta\alpha + \mathbf{c}_a \geq \mathbf{0}, \\ &\Delta\mathbf{z}_a \geq \mathbf{0},\ \mathbf{w}_a^{\mathrm{T}}\Delta\mathbf{z}_a = 0, \end{aligned} \tag{35}$$

where

$$\bar{\mathbf{z}}_b + \Delta\mathbf{z}_b \geq \mathbf{0}. \tag{36}$$

In the present case, $\Delta\mathbf{z}_b$ is sign unconstrained. This allows the yield functions in $\{b\}$ to stay active (at yield) while the associated plastic multipliers $\mathbf{z}_b$ can decrease in a reversible fashion, provided that Eq. 36 is satisfied.

At variance with the geometrically linear problem, the governing vectors **b**, **c** and matrix **A** contain nonlinear components, namely **S**, **K**, **Z** for the 2nd-order geometric problem. This requires the use of iterative procedures to achieve convergence. The basic approach is to approximate actual nonlinear quantities, for each iteration, by using previously found solutions as data to form equivalent linear functions. The minimum time step Δt is then iteratively calculated from an identification of either an activation of new yield planes Δt_a, exhaustion of plastic multipliers Δt_b or a preset step Δt_p that should be small enough to accurately trace the nonlinear structural behavior.

The iterative procedures used are basically as follows:

1. Check convergence criterion: if $\max(abs(\mathbf{s}_i - \mathbf{s}_{i-1})) \leq tol$ (e.g. 10^{-6}), then terminate. Else, go to Step 2.

2. If $\mathbf{f}_d$ is involved, go to Step 3. Else, set $\Delta\alpha_i = (\Delta\alpha_{i-1}/\Delta t_{i-1})\Delta t_i$, $\Delta\mathbf{z}_i = (\Delta\mathbf{z}_{i-1}/\Delta t_{i-1})\Delta t_i$, and recalculate $\mathbf{s}_i$. Then, go to Step 3.

3. Set $i = i+1$. Assume that $\mathbf{s}_i = \mathbf{s}_{i-1}$, and calculate the new $\mathbf{S}$, $\mathbf{K}$, $\mathbf{Z}$ as required for the 2nd-order geometry case.

4. If $\mathbf{f}_d$ is present, go to Step 5. Else, go to Step 6.

5. Use the elastic constitutive law to calculate relevant response variables (e.g. $\mathbf{s}_i$ and $\mathbf{w}_i$) when subjected to $\mathbf{f}_d$ alone (i.e. $\alpha_i = 0$ and $\mathbf{z}_i = \mathbf{0}$). Repeat Step 1.

6. At the known stress state $\bar{\Sigma}$, calculate $\mathbf{A}$, $\mathbf{b}$, $\mathbf{c}$, $\bar{\mathbf{w}}_p$ using Eq. 34. If $\{a\} \cup \{b\}$ is empty, go to Step 7. Else, go to Step 8.

7. Solve Eq. 33 for $\Delta\alpha_i = \Delta\alpha_{i-1}$. Go to Step 10.

8. Formulate the corresponding $\mathbf{A}_{aa}$, $\mathbf{A}_{ab}$, $\mathbf{A}_{bb}$, $\mathbf{A}_{ba}$, $\mathbf{b}_a$, $\mathbf{b}_b$, $\mathbf{c}_a$, $\mathbf{c}_b$.

9. Solve Eq. 35 for $\Delta\alpha_i = \Delta\alpha_{i-1}$.

10. Update as usual: $\alpha_i = \bar{\alpha} + \Delta\alpha_i$, $\mathbf{z}_i = \bar{\mathbf{z}} + \Delta\mathbf{z}_i$, $\mathbf{w}_i = \mathbf{A}\Delta\mathbf{z}_i - \mathbf{b}\Delta\alpha_i + \mathbf{c}$. Calculate the new $\mathbf{s}_i$.

11. Compute the new time step Δt_i at the load factor $\bar{\alpha} + (\Delta\alpha_{i-1}/\Delta t_{i-1})\Delta t_i$ from the following linear predictions:

$$\Delta t_a = \min\left\{ \frac{\Delta t_{i-1}(\bar{\mathbf{w}}_p)_j}{(\mathbf{N}^{\mathrm{T}}(\mathbf{s}_i - \bar{\mathbf{s}}) - \mathbf{H}\Delta\mathbf{z}_i)_j} \right\} > 0, \quad \text{for all } j \in \{p\}, \tag{37}$$

$$\Delta t_b = \min\left\{ \frac{\Delta t_{i-1}(\bar{\mathbf{z}}_b)_k}{(-\Delta\mathbf{z}_i)_k} \right\} > 0, \text{ for all } k \in \{b\}, \tag{38}$$

$$\Delta t_i = \min\{\Delta t_a, \Delta t_b, \Delta t_p\}. \tag{39}$$

Then, repeat Step 1.

The overall algorithm is outlined in the following. Note that whilst the procedure correctly identifies which hinges wish to elastically unload at Step (c), the holonomic formulation precludes this from happening.

Step (0): Initialization

- Set stopping criterion: load level, maximum number of equilibrium paths, etc.
- Define the preset step Δt_p, which is a positive constant value.
- Initialize variables (e.g. $\alpha = 0$, $\mathbf{s} = \mathbf{0}$, $\mathbf{z} = \mathbf{0}$ and $\mathbf{w} = \mathbf{r}$). Go to Step (a).

Step (a): Account for fixed loads

- If fixed loads $\mathbf{f}_d = \mathbf{0}$, go to Step (b).
- Else, at $i = 1$, initialize $\mathbf{s}_{i-1} = \mathbf{0}$.
- Assume initially that $\mathbf{s}_i = \mathbf{s}_{i-1}$. Calculate $\mathbf{S}$, $\mathbf{K}$, $\mathbf{Z}$ relevant to the 2nd-order geometry case.
- Use the elastic constitutive law to calculate relevant response variables (e.g. $\mathbf{s}_i$ and $\mathbf{w}_i$) when subjected to $\mathbf{f}_d$ alone (i.e. $\alpha_i = 0$ and $\mathbf{z}_i = \mathbf{0}$). Then, iterate until convergence using iterative procedures.
- Form the new stress state $\bar{\Sigma}$, and update the following: $\alpha = \alpha_i$, $\mathbf{s} = \mathbf{s}_i$, $\mathbf{z} = \mathbf{z}_i$ and $\mathbf{w} = \mathbf{w}_i$. Go to Step (b).

Step (b): Process empty active set

- At $i = 1$, initialize $\Delta t_{i-1} = \Delta t_p$, $\Delta \alpha_{i-1} = \Delta t_{i-1}$ and $\mathbf{s}_{i-1} = \bar{\mathbf{s}}$.
- Assume that $\mathbf{s}_i = \mathbf{s}_{i-1}$. Calculate $\mathbf{S}$, $\mathbf{K}$, $\mathbf{Z}$ relevant to the 2nd-order geometry case.
- At this known stress state $\bar{\Sigma}$, the structure contains solely inactive stresses. Calculate $\mathbf{A}$, $\mathbf{b}$, $\mathbf{c}$, $\bar{\mathbf{w}}_p$ using Eq. 34.
- Solve Eq. 33 for $\Delta \alpha_i = \Delta \alpha_{i-1}$. Then, go to Step (d).

Step (c): Process active set

- At $i = 1$, initialize $\Delta t_{i-1} = \Delta t_p$ and $\mathbf{s}_{i-1} = \bar{\mathbf{s}}$.
- Assume that $\mathbf{s}_i = \mathbf{s}_{i-1}$. Calculate $\mathbf{S}$, $\mathbf{K}$, $\mathbf{Z}$ relevant to the 2nd-order geometry case.
- At the known stress state $\bar{\Sigma}$, calculate $\mathbf{A}_{aa}$, $\mathbf{A}_{ab}$, $\mathbf{A}_{bb}$, $\mathbf{A}_{ba}$, $\mathbf{b}_a$, $\mathbf{b}_b$, $\mathbf{c}_a$, $\mathbf{c}_b$, $\bar{\mathbf{w}}_p$ using Eq. 34.
- Solve Eq. 35 for two load increments of $\Delta\alpha_i = \Delta\alpha_{i-1}$, where $\Delta\alpha_{i-1} = \Delta t_p$ and $\Delta\alpha_{i-1} = -\Delta t_p$, respectively.
- Collect all multiple solutions, if any. Choose one solution and go to Step (d).

Step (d): Identify activation

- Update: $\alpha_i = \bar{\alpha} + \Delta\alpha_i$, $\mathbf{z}_i = \bar{\mathbf{z}} + \Delta\mathbf{z}_i$, $\mathbf{w}_i = \mathbf{A}\Delta\mathbf{z}_i - \mathbf{b}\Delta\alpha_i + \mathbf{c}$. Calculate the new $\mathbf{s}_i$.
- Compute the new time step Δt_i from the three linear Eqs. 37-39. Then, iterate until convergence using iterative procedures.
- Form the new stress state $\bar{\Sigma}$, and update the following: $\alpha = \alpha_i$, $\mathbf{s} = \mathbf{s}_i$, $\mathbf{z} = \mathbf{z}_i$ and $\mathbf{w} = \mathbf{w}_i$. Go to Step (e).

Step (e): Check termination

- If the termination criterion has been reached, or all solutions found at Step (c) have been exhausted, stop.
- Else if $\{a\} \cup \{b\}$ is empty, return to Step (b) to continue with this empty active set in the known state $\bar{\Sigma}$.
- Else, return to Step (c) to proceed with the current state $\bar{\Sigma}$ or to choose a stored, as yet unexplored, solution found previously.

Two remarks are worth noting:

(a) As bifurcation, leading to multiple equilibrium paths, can exist at any load step, the algorithm attempts to capture all of them by processing Step (c) for both $\Delta\alpha_i = \Delta t_p$ and $\Delta\alpha_i = -\Delta t_p$. This is achieved through a variant of the special scheme [Tin-Loi and Tseng (2003); Tin-Loi, Tangaramvong, and Xia (2007)] to search for all

multiple solutions at Step (c). For large structures, such a step-by-step analysis, as expected, can be computationally demanding especially if key events such as new plastic activations need to be captured exactly. Fortunately, it is invariably the case that, for practical structures, multiple equilibrium paths do not exist [Tangaramvong and Tin-Loi (2007a)].

(b) For the 2nd-order geometrically nonlinear case, a small preset step Δt_p helps the iterative procedures to converge. From our numerical experience, this event-by-event holonomic algorithm handles well problems involving 2nd-order geometry effects. Not only are all the critical events, such as limit points, identified exactly, but also such instability phenomena as postpeak and snapback behaviors can be mapped out. The convergence to each solution typically requires only a small number of iterative resources to terminate.

4 Limit analysis under ductility constraints

The aim forming the focus of this section, indeed of the present paper, is to compute an upper bound on the limit load of the structure for which given ductility constraints are also satisfied. Various other quantities of interest, such as the corresponding displacements $\mathbf{u}$ and stresses $\mathbf{s}$, will be obtained as a by-product. The immediate practical application of this one-step analysis is in the safety assessment of, for example, steel frames with softening constitutive laws; of structures with low ductility reinforced concrete beams that have limited rotation capacities; and of structures for which displacements at some specific points are limited.

The proposed approach is conceptually simple especially since the holonomic formulation given by Eq. 26 provides all key ingredients that govern the structural behavior for the entire proportionally applied load history. The very same relations can be used to set up the extended limit analysis problem for finding the maximum load. At variance with a holonomic analysis for which the load multiplier α is known, the limit analysis assumes that α is a variable. In particular, the aim is to maximize α subject to the indicated constraints. Therefore, the proposed approach involves solving the following optimization problem in variables $(\alpha, \mathbf{s}, \pi_f, \mathbf{u}, \mathbf{z})$:

$$\begin{array}{ll} \text{maximize} & \alpha \\ \text{subject to} & \mathbf{C}_0^{\mathrm{T}}\mathbf{s} + \mathbf{C}_f^{\mathrm{T}}\pi_f - \alpha\mathbf{f} - \mathbf{f}_d = \mathbf{0}, \\ & \mathbf{S}^{-1}\mathbf{s} - \mathbf{C}_0\mathbf{u} + \mathbf{N}\mathbf{z} = \mathbf{0}, \\ & \mathbf{S}_f^{-1}\pi_f - \mathbf{C}_f\mathbf{u} = \mathbf{0}, \\ & \mathbf{w} = -\mathbf{N}^{\mathrm{T}}\mathbf{s} + \mathbf{H}\mathbf{z} + \mathbf{r} \geq \mathbf{0},\ \mathbf{z} \geq \mathbf{0},\ \mathbf{w}^{\mathrm{T}}\mathbf{z} = 0, \\ & \text{ductility constraints.} \end{array} \tag{40}$$

The general constraint set labeled "ductility constraints" in Eq. 40, is used to impose limits on such quantities as rotation capacities and total displacements at some

specific points of structures.

The problem given by Eq. 40 is an MPEC [Luo, Pang, and Ralph (1996)]. In our case, the equilibrium constraints are in fact complementarity constraints.

The systematic study of MPECs is a relatively new field in mathematical programming, even though they appear to have originated as early as the 1970s in the form of so-called "bilevel" programs. This class of optimization problems has increasingly attracted research interest due to the fact that, in addition to being theoretically difficult and computationally challenging, MPECs find numerous applications in economic and engineering problems involving equilibrium systems [Ferris and Pang (1997)].

There are three main reasons why an MPEC such as the one given by Eq. 40 is extremely difficult to solve [Luo, Pang, and Ralph (1996)]. Firstly, as is well-known from the integer programming literature, disjunctive constraints such as those embodied by the complementarity conditions (namely, either $w_j = 0$ or $z_j = 0$) are very difficult to handle. This, as a result, makes the MPEC disjunctive. More explicitly, there is no feasible point for which all inequalities are strictly satisfied. Even under restrictions, this makes the feasible region a union of finitely many closed sets. Secondly, the feasible region of the MPEC may not be convex, so that the MPEC itself is not convex. This implies that an MPEC may contain more than one local minimizer. Finally, the feasible solution space of the MPEC may not even be connected. Any subset of the above three difficulties often occurs and is expected to show up as a severe numerical instability. Therefore, it is not surprising than MPECs are said to be ill-posed.

In spite of these various difficulties, the authors have had considerable success in solving similar MPECs, e.g. Tangaramvong and Tin-Loi (2007b). Our strategy is to attempt solving the reformulated MPEC given by Eq. 40 as a standard NLP problem, after suitably treating the complementarity conditions. Various techniques that can be adopted to achieve this are outlined in the next section.

Before presenting these approaches, it should be mentioned that the governing formulations of the 2nd-order geometry problem (as discussed earlier) contain two matrices $\mathbf{S}$ and $\mathbf{S}_f$ involving unknown stresses $\mathbf{s}$. A series of iterative MPEC solves are thus required. The basic iterative procedure is as follows:

1. At $i = 0$, initialize $\mathbf{s}_i = \mathbf{0}$.

2. Set $i = i + 1$. Assume that $\mathbf{s}_i = \mathbf{s}_{i-1}$, and calculate the new $\mathbf{S}$ and $\mathbf{S}_f$. Then, formulate Eq. 40.

3. Solve Eq. 40. Obtain new solution sets for α_i, $\mathbf{s}_i$, $\pi_{f,i}$, $\mathbf{u}_i$ and $\mathbf{z}_i$.

4. Check convergence criterion: if $\max(abs(\mathbf{s}_i - \mathbf{s}_{i-1})) \leq tol$ (e.g. 10^{-6}), then terminate. Else, repeat Step 2.

5 NLP based approaches

An attempt to directly solve the MPEC given by Eq. 40 is likely to succeed only for small-size problems, and not for realistic (often large-size) structures. A far better approach, as is presented in this section, is to parameterize the nonconvex complementarity constraints such that the original complementarity condition is approached, as the governing parameter is increased or decreased. More explicitly, the reformulated MPEC is solved as a series of NLP subproblems that aim to increasingly achieve complementarity. The attraction of this scheme, it should be noted, is that each subproblem is a standard NLP problem, and general purpose NLP codes such as GAMS/CONOPT [Drud (1994)] can be used.

In the following, three basic algorithms, essentially categorized by the way in which complementarity is reformulated, are proposed for solving the MPEC given by Eq. 40, where μ is a positive parameter used to enforce complementarity.

(a) *Penalization*: The penalty algorithm has been successfully used in the context of minimum weight design [Ferris and Tin-Loi (1999)] as well as for quasibrittle fracture parameter identification [Tin-Loi and Que (2002)]. The basic idea is that the complementarity term is transferred to the objective function and penalized. In particular, this involves adding the term $-\mu \mathbf{w}^{\mathrm{T}}\mathbf{z}$ to the objective function; a negative penalization is necessary in view of a maximization requirement. The algorithm then increases the penalty parameter μ at each NLP iterate with the intention of driving the complementarity term to zero.

(b) *Fischer-Burmeister smoothing*: The smoothing algorithm has been successfully used for the solution of MPECs that arise in some minimum weight problems [Tin-Loi (1999)]. The idea is to replace the complementarity conditions by the set of smoothing equations $\varphi_\mu(w_j, z_j) = 0$ for all j. The particular φ_μ function used is the well-known Fischer-Burmeister function [Kanzow (1996)]

$$\varphi_\mu(w_j, z_j) = \sqrt{w_j^2 + z_j^2 + 2\mu} - (w_j + z_j). \tag{41}$$

This function φ_μ has the property that $\varphi_\mu(w_j, z_j) = 0$ if and only if $w_j \geq 0$, $z_j \geq 0$, $w_j z_j = \mu$. The parametrization φ_μ is a smoothing of the mapping $\varphi_{\mu=0}$ implying that it is differentiable for nonzero μ. The algorithm then consists of solving a series of NLP subproblems that iteratively decrease the smoothing parameter μ in order to drive the complementarity term to zero.

(c) *Relaxation*: The relaxation method has been successfully used in the collapse load evaluation of block assemblies in frictional contact [Ferris and Tin-Loi (2001)]. The key idea consists in replacing the original complementarity constraints $\mathbf{w}^{\mathrm{T}}\mathbf{z}=0$ by the relaxed constraints $\mathbf{w}^{\mathrm{T}}\mathbf{z}\leq\mu$. Consequently, the algorithm solves a series of NLP subproblems for successively smaller values of μ until the complementarity condition is satisfied.

All these three NLP based approaches had no difficulty whatsoever in solving the MPEC described by Eq. 40 for all the problems tested. The penalty approach, in view of its noticeably better robustness, is the preferred scheme. The particular algorithmic implementation of the penalty approach is straightforward. The penalty subproblem

$$\begin{array}{ll}\text{maximize} & \alpha-\mu\mathbf{w}^{\mathrm{T}}\mathbf{z}\\ \text{subject to} & \mathbf{C}_0^{\mathrm{T}}\mathbf{s}+\mathbf{C}_f^{\mathrm{T}}\pi_f-\alpha\mathbf{f}-\mathbf{f}_d=\mathbf{0},\\ & \mathbf{S}^{-1}\mathbf{s}-\mathbf{C}_0\mathbf{u}+\mathbf{N}\mathbf{z}=\mathbf{0},\\ & \mathbf{S}_f^{-1}\pi_f-\mathbf{C}_f\mathbf{u}=\mathbf{0},\\ & \mathbf{w}=-\mathbf{N}^{\mathrm{T}}\mathbf{s}+\mathbf{H}\mathbf{z}+\mathbf{r}\geq\mathbf{0},\ \mathbf{z}\geq\mathbf{0},\\ & \text{ductility constraints.}\end{array}\tag{42}$$

is processed in accordance with the following pseudocode:

- Set: initial μ (e.g. 0.1), maximum iterations ($maxiter$), and $\mathbf{w}^{\mathrm{T}}\mathbf{z}=100$.
- For $k=1$ to $maxiter$
  if $\mathbf{w}^{\mathrm{T}}\mathbf{z}\leq 10^{-6}$, then exit
  solve Eq. 42
  increase μ (e.g. $\mu=10\mu$)
  end.

As indicated earlier, Eq. 42 is solved for successively higher values of μ until a preset tolerance on the complementarity condition (e.g. $\mathbf{w}^{\mathrm{T}}\mathbf{z}\leq 10^{-6}$) has been met. Typical starting values of μ are within the range 0.1-1, with an update of $\mu=10\mu$ after each NLP solve. A good specification of initial variables (e.g. $\mathbf{w}=\mathbf{r}$) often helps in solving the NLP problems.

6 Illustrative examples

Three numerical examples are provided to illustrate application of the proposed extended limit analysis approach. For each of the three examples, four analysis cases have been run as follows:

Case a: Holonomic analysis, perfectly plastic, geometric linearity.

Case b: Holonomic analysis, softening, geometric linearity.

Case c: Holonomic analysis, softening, 2nd-order geometric nonlinearity.

Case d: Extended limit analysis, softening, 2nd-order geometric nonlinearity.

The primary aims of this study were as follows. Firstly, the justification of the proposed limit analysis approach Case d is revealed by using the associated holonomic response Case c. Secondly, the effects of softening instability can be assessed through a comparison of the softening Case b with the perfectly plastic Case a. Finally, the necessity to include the effects of geometry changes is assessed by comparing the results of the 2nd-order geometry Case c with those of the geometrically linear Case b.

In all cases, positive and negative yield properties were assumed to be identical. Moreover, the parameters adopted in Fig. 5 were: $r_b = 0.15$, $\tan\gamma = 1/0.85$, $a_j = 1$ for all j, and $p_c = p_{c1}$. For a perfectly plastic hinge a, the yield functions $w1$ to $w6$, as expressed in Eq. 22, were used, with the softening parameter h set to zero leading to $\mathbf{H}^a = \mathbf{0}$.

The proposed extended limit analysis has been implemented as a MATLAB code. The code sets up appropriate text files for the MPEC algorithm developed, namely penalty algorithm, and is interfaced with GAMS using the MATLAB-GAMS environment [Ferris (1998)]. The GAMS/CONOPT solver [Drud (1994)] was chosen in view of its robustness. In the MPEC runs, parameter μ was updated at every iteration by $\mu = 10\mu$; the initial $\mu = 0.1$ for Example 1; $\mu = 1$ for Examples 2 and 3. Computational times are not reported since the various MPEC solves took only a few seconds to process all problems.

For the holonomic runs, the event-by-event holonomic algorithm described was adopted to trace complete responses for the structures considered. The code was again developed within the MATLAB and GAMS environments. GAMS/PATH [Dirkse and Ferris (1995)] was used as the MCP solver.

6.1 Example 1: Single bay eccentrically braced frame

The three story, single bay eccentrically braced frame shown in Fig. 6, with the same geometry as in Karakostas and Mistakidis (2000), was analyzed. The frame was subjected to vertical and horizontal loads (kN) controlled by load factor α; v denotes the top right story sway displacement (m).

The discrete structural model consisted of 21 elements, 14 nodes and 36 degrees of freedom. Steel with $E = 2 \times 10^8$ kNm^{-2} was assumed. The particular sections employed were: 310UC118 for all columns, $s_{2u} = 548.80$ kNm, $s_{1u} = 4200$ kN; 200UB18.2 for all beams, $s_{2u} = 57.60$ kNm, $s_{1u} = 742.40$ kN; SHS125/125/9 for all

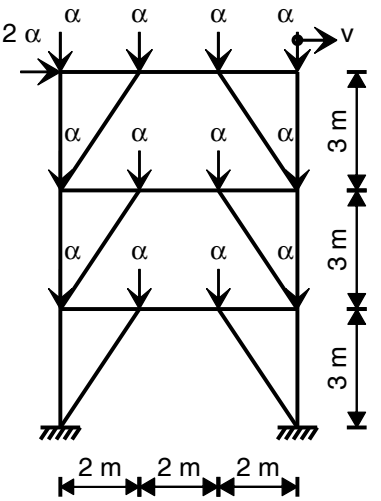

Figure 6: Example1: single bay eccentrically braced frame.

bracings, $s_{2u} = 57.75$ kNm, $s_{1u} = 1365$ kN. In all runs, bracing members were assumed to be made of a perfectly plastic material. For the softening runs, the simple bilinear softening model of Fig. 5 was adopted. In particular, it was assumed that: for all columns, $h = -202.79$ kNm, $r_r = 0.7$; and for all beams, $h = -41.04$ kNm, $r_r = 0.7$.

In all Cases a to c, only a single equilibrium path was identified, as expected of practical structures. These holonomic responses are compared in Fig. 7, namely Case a (dashed line), Case b (dashed dot line) and Case c (solid line). The extended limit analysis Case d was successfully solved after a total of 15 MPEC iterates. In particular, the maximum load computed, namely $\alpha_{\max} = 102.283$ with $v = 0.269$ m, is plotted as a dot on the associated holonomic Case c response in Fig. 7. The collapse load $\alpha_{\text{col}} = 124.148$ obtained from a classical limit analysis (about 21% higher than the load considering softening and 2nd-order geometric nonlinearity) is also shown as a dotted line in Fig. 7. Hinge dispositions at the maximum loading states for all cases are drawn in Fig. 8. Identical hinge dispositions were obtained for Cases c and d.

For the geometrically linear Cases a and b, the initial elastic responses were identical until $\alpha = 57.853$ when some beam section started to yield. The subsequent progress was then as follows.

In Case a, some further perfectly plastic hinges formed in various beams. When

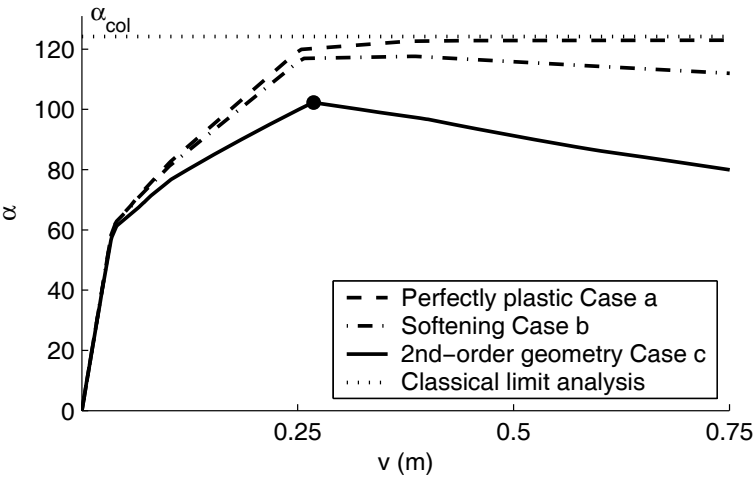

Figure 7: Example1: holonomic $\alpha - v$ responses.

$\alpha = 118.478$ and $\alpha = 119.921$, two consecutive hinges appeared respectively at base columns due to the heavy axial forces applied. Then, a bracing member started to yield at $\alpha = 122.616$, followed by another at $\alpha = 122.639$. The analysis was stopped at $v = 0.75$ m when $\alpha = 122.982$.

In Case b, softening hinges initially formed at beam sections. Two column hinges were respectively formed at $\alpha = 115.789$ and $\alpha = 116.932$. The maximum load was approached at $\alpha = 117.617$ when the bottom bracing started to form a perfectly plastic hinge. Clearly, the presence of softening behavior led to some reduction (about 5%) in the load carrying capacity of the structure as compared with the perfectly plastic assumption Case a.

The 2nd-order geometry Case c was solved by using the proposed iterative procedures, in which a preset step $\Delta t_p = 5$ was applied throughout. In Fig. 7, the overall structural behavior of this Case c showed yielding at increased load but reduced stiffness initially and then softening after the limit point. As expected, some deviation from the small deformation Case b was noticed early due to the effects of geometric nonlinearity. The load capacity of the Case c was found to be lower than that of Case b. In particular, first yield was reached at some beam section when $\alpha = 56.586$. This was followed by the successive activation of softening hinges at some other beams, until at $\alpha = 101.992$ when a softening hinge was formed at some base column. In contrast to the small deformation Case b in which the peak load was attained by yielding of some bracing, the limit point of this 2nd-order geome-

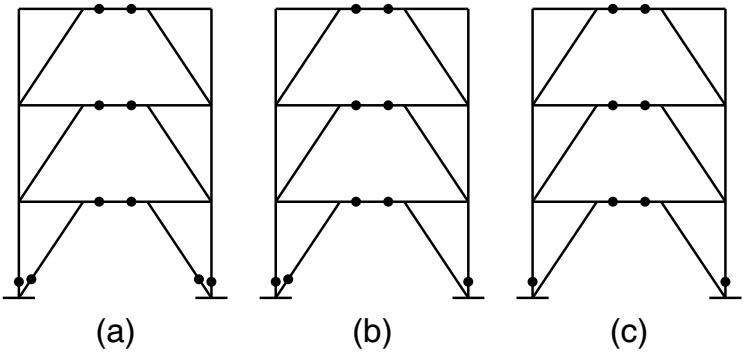

Figure 8: Example1: hinge dispositions at limit load (a) Case a, (b) Case b, (c) Cases c and d (• denotes hinge on perfectly plastic or descending yield branch).

try Case c was reached earlier by yielding at another base column at $\alpha = 102.283$, some 15% less than that of Case b. Clearly, accounting for geometric nonlinearity is significant as it indicated collapse of the structure at a lower load factor than the prediction of a small deformation analysis. Interestingly, pseudo-mechanisms, indicating configuration changes within a constant load level [Maier, Giacomini, and Paterlini (1979)], were found during the postpeak behaviors in both Cases b and c. These were efficiently handled by the computational strategies implemented; see Tangaramvong and Tin-Loi (2007a) for details.

6.2 Example 2: Nine story portal frame

The nine story portal frame shown in Fig. 9 was subjected to the increasing vertical point loads of 6α (kN) and increasing lateral loads (kN) governed by load factor α; v denotes the corresponding top story sway displacement (m). In this example, the ductility constraints applied were limits on the sway displacement of $-0.148 \leq v \leq 0.148$ (m). The structure was discretized into 126 elements, 93 nodes, 261 degrees of freedom and 213 critical sections (at column ends, beam ends and mid-span).

Steel sections with $E = 2 \times 10^8$ kNm^{-2} were adopted: 400WC328 for all columns ($s_{2u} = 1988$ kNm, $s_{1u} = 11704$ kN) and 460UB82.1 for all beams ($s_{2u} = 552$ kNm, $s_{1u} = 3150$ kN). For the softening Cases b to d (Fig. 5), the parameters employed were: for columns $h = -18418.78$ kNm, $r_r = 0.7$; for beams $h = -4852.04$ kNm at beam ends, $h = -2426.02$ kNm at mid-span, $r_r = 0.7$.

As in the previous Example 1, the holonomic responses in Fig. 10 of each case,

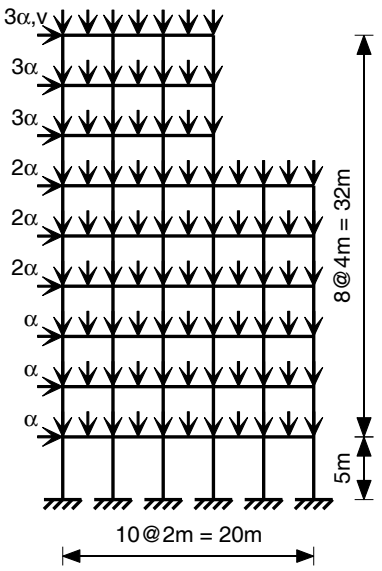

Figure 9: Example 2: nine story portal frame.

namely Case a (dashed line), Case b (dashed dot line) and Case c (solid line), exhibited only a single equilibrium path. The extended displacement constrained limit analysis Case d was successfully solved in 12 MPEC iterates. The maximum load computed, namely $\alpha_{\max} = 58.960$ with $v = 0.148$ m, is plotted as a dot on the associated holonomic behavior Case c in Fig. 10. This result clearly satisfies the imposed displacement constraint (thin line). Hinge dispositions at the peak load for all cases are plotted in Fig. 11. A classical (rigid perfectly plastic) limit analysis approach, it should be noted, estimated a far higher collapse load, namely $\alpha_{\text{col}} = 93.724$ (dotted line in Fig. 10), than that predicted in Case d.

In the small deformation Cases a and b, the initial elastic responses were similar. When $\alpha = 55.359$ and 55.374, first and second hinges formed respectively at some beam sections. In Case a, a column section first yielded at $\alpha = 69.981$. The analysis was terminated at $\alpha = 91.754$ with $v = 0.75$ m. In Case b, the first column hinge formed at $\alpha = 69.351$. The maximum load was attained at $\alpha = 79.709$, approximately 15% less than that of the perfectly plastic Case a. The corresponding hinge formations (Fig. 11) showed that all column hinges were formed due to the effects of both softening and combined stresses.

In the 2nd-order geometry Case c, the iterative procedures were used with a preset step of $\Delta t_p = 5$. As shown in Fig. 10, the overall load behavior showed a weaker

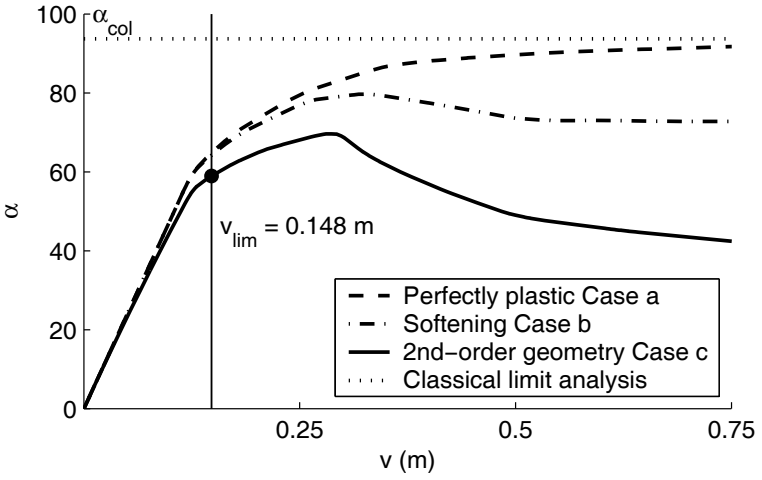

Figure 10: Example 2: holonomic $\alpha - v$ responses.

structure than that of the small deformation Case b. The responses of two Cases b and c started to differ in the early elastic state. Not only was a smaller maximum load attained for Case c, but the postpeak behavior also showed a sharper drop, as when compared to Case b. More specifically, beams and columns developed their first hinge at $\alpha = 51.949$ and 65.167, respectively. The maximum load was reached at $\alpha = 69.616$, some 15% less than that of Case b. The corresponding hinge dispositions (Fig. 11) also showed that some beam and column hinges previously reported for Case b did not form in Case c. This implies that Case b has provided an unsafe prediction since geometric nonlinearity has been neglected.

6.3 Example 3: Fourteen story braced frame

The last example concerns the practical braced frame shown in Fig. 12. This fourteen story frame was subjected to increasing vertical loads of 5α (kN) as well as lateral loads (kN) governed by the load factor α as shown; v denotes the corresponding top sway displacement (m). This sway displacement was further limited, for serviceability reasons, to $-0.224 \leq v \leq 0.224$ (m).

The adopted model consisted of 196 members, 130 nodes and 378 degrees of freedom. Steel sections with $E = 2 \times 10^8$ kNm^{-2} were employed as follows: 350WC258 for all columns, $s_{2u} = 1246$ kNm, $s_{1u} = 9212$ kN; 410UB59.7 for all beams, $s_{2u} = 360$ kNm, $s_{1u} = 2292$ kN; and 200UC59.5 for all braces, $s_{2u} = 197$ kNm, $s_{1u} = 2286$ kN. For the softening cases, the yield model shown in Fig. 5

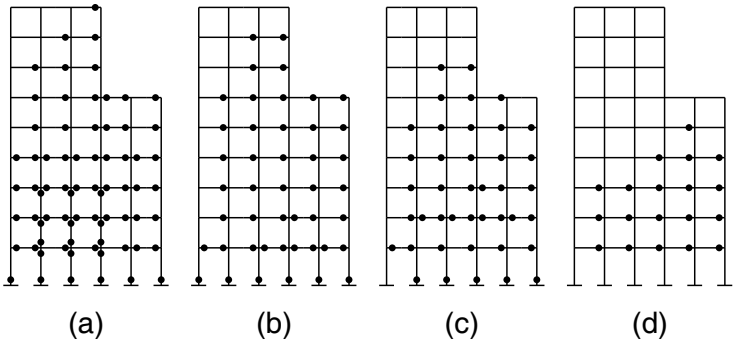

Figure 11: Example 2: hinge dispositions at limit load (a) Case a, (b) Case b, (c) Case c and (d) Case d (• denotes hinge on perfectly plastic or descending yield branch).

was adopted with the following parameters: for all columns, $h = -11435$ kNm, $r_r = 0.7$; for all beams, $h = -3192$ kNm at beam ends, $h = -1596$ kNm at interval-span load points, $r_r = 0.7$; and for all braces, $h = -1748$ kNm, $r_r = 0.7$.

As is expected of realistic structures, the holonomic behaviors in Fig. 13 of each case, namely Case a (dashed line), Case b (dashed dot line) and Case c (solid line), exhibited, as in the previous examples, a single equilibrium path. However, at variance with these two previous examples, the holonomic responses of the softening Cases b and c showed physically unstable snapback behaviors. This is evidenced by a reduction in load factor at the same time as a decrease of the sway displacement. Moreover, these softening responses exhibited two local maximum loads.

In Fig. 13, the extended limit analysis approach (Case d) captured exactly the maximum load factor of $\alpha_{\max} = 37.890$ at $v = 0.089$ m after 6 MPEC solves. Fig. 13 validates our single-step limit analysis approach which clearly shows that the maximum load (plotted as a dot on its associated holonomic Case c behavior) has been exactly computed and also that the corresponding displacement v has satisfied the serviceability limit (thin line). A classical limit analysis (dotted line in Fig. 13) again provided a higher collapse load estimation of $\alpha_{\text{col}} = 48.293$. Hinge dispositions at peak load for all cases are displayed in Fig. 14.

The initial elastic responses of the two geometrically linear Cases a and b were identical. They started to differ, as a result of the difference in material properties, after $\alpha = 36.713$, coinciding with first yield at some base column. This was then followed by yielding of various cross-sections, as detailed in the following.

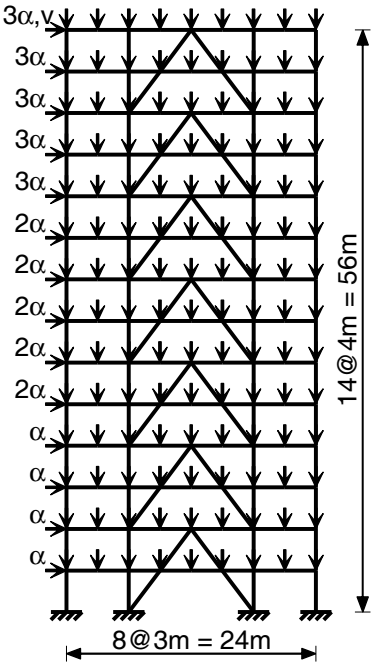

Figure 12: Example 3: fourteen story braced frame.

In Case a, the load factor kept increasing with further yielding at columns until $\alpha = 40.112$, where some beam formed its first perfectly plastic hinge. Yielding at columns and beams continued with the increase in load factor, but decrease in stiffness. The bottom brace hinge formed at $\alpha = 42.684$. The holonomic analysis Case a was terminated when $v = 0.75$ m and $\alpha = 47.359$.

In Case b, the maximum load was attained at $\alpha = 38.141$, some 24% less than that of Case a, after yielding of some column. Then, the load factor dropped sharply with holonomic reversal of plastic strains at columns, thus leading to the snapback equilibrium path. The load capacity was recovered by yielding of two consecutive softening hinges formed in a beam and a brace at $\alpha = 31.146$ and 33.841, respectively. The second peak load was reached at $\alpha = 35.120$, just prior to another softening of the equilibrium path.

The 2nd-order geometrically nonlinear Case c analysis was carried out using a preset step of $\Delta t_p = 5$. As compared to the linear Case b, the effect of geometric nonlinearity reduced only slightly the overall load capacity of the structure. However, this effect was more significant as the displacement v increased. Thus, the

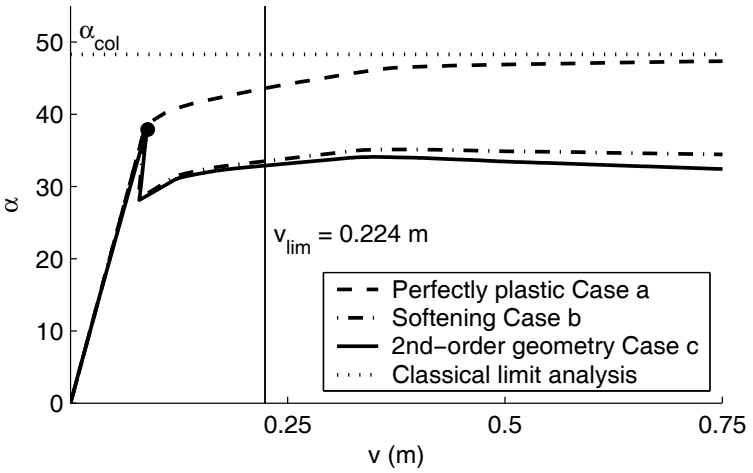

Figure 13: Example 3: holonomic $\alpha - v$ responses.

first yield at some column section was reached at $\alpha = 36.513$. The maximum load was attained at $\alpha = 37.890$, approximately 1% less than that of Case b. Softening hinges formed at some beam and brace when $\alpha = 30.844$ and $\alpha = 33.244$, respectively. Finally, the second peak load was reached at $\alpha = 34.084$.

7 Concluding remarks

An extended limit analysis approach, suitable for plane frames accounting for the effects of 2nd-order geometric nonlinearity and limited ductility, has been developed. The material model adopted can accommodate the effect of local softening instability, for which plasticity can be caused by interaction of flexural and axial forces. The scheme can simultaneously compute an upper bound to the limit load, and the corresponding deformations and stresses. As with classical limit analyses, the computation is performed in a single-step fashion, without the need for step-by-step evolutive analyses. In this respect, the extended limit analysis computation represents a useful, simplified analysis for preliminary safety assessment or design.

The formulation of the extended limit analysis takes the form of a notoriously difficult to solve instance of a nonconvex and nonsmooth optimization problem known as an MPEC. Reformulation of this MPEC into a standard NLP problem allows robust and efficient solution of the MPEC. Various ways of achieving this reformulation has been described. The one adopted, in view of its superiority, is a penalty based approach.

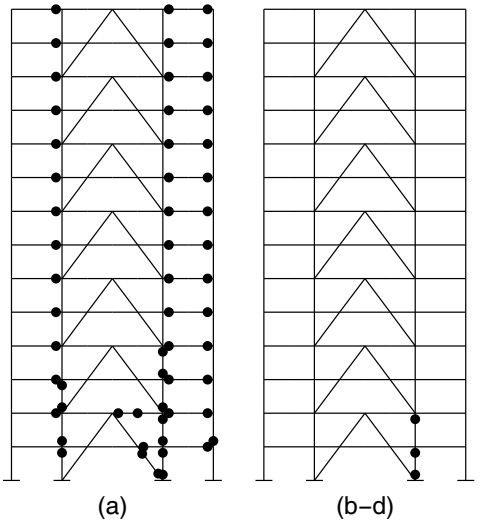

Figure 14: Example 3: hinge dispositions at limit load (a) Case a, (b) Cases b to d (• denotes hinge on perfectly plastic or descending yield branch).

A number of numerical examples concerning practical, reasonably sized structures are presented to illustrate application and validity of the proposed approach, as well as to highlight the effects of softening and geometric nonlinearities. A number of pertinent observations can be made. Firstly, when there exists, as is typical of realistic frames, only a single equilibrium path, the upper bound solution is in effect the exact limit load solution. Secondly, the effects of both local softening and geometric nonlinearities need to be taken into account for the realistic analysis of structures, since any of these can reduce not only the overall load carrying capacity but also the postpeak ductility. Thirdly, accounting for any limited ductility exhibited by structures is essential, since ignoring such limitations often leads to violations of some serviceability requirement or even to a premature failure of the structure.

Acknowledgement: This research was supported by the Australian Research Council through ARC Discovery Grant DP0986332.

References

Ardito, R.; Cocchetti, G.; Maier, G. (2008): On structural safety assessment by load factor maximization in piecewise linear plasticity. *European Journal of*

Mechanics A−Solids, vol. 27, pp. 859–881.

Armero, F.; Ehrlich, D. (2006): Numerical modeling of softening hinges in thin Euler-Bernoulli beams. *Computers and Structures*, vol. 84, pp. 641–656.

Bolzon, G.; Corigliano, A. (1997): A discrete formulation for elastic solids with damaging interfaces. *Computer Methods in Applied Mechanics and Engineering*, vol. 140, pp. 329–359.

Bolzon, G.; Tin-Loi, F. (1999): Physical instability and geometric effects in frames. *Engineering Structures*, vol. 21, pp. 557–567.

Brooke, A.; Kendick, D.; Meeraus, A.; Raman, R. (1998): *GAMS: a user's guide*. Gams Development Corporation, Washington DC.

Carvelli, V.; Maier, G.; Taliercio, A. (2000): Kinematic limit analysis of periodic heterogeneous media. *CMES: Computer Modeling in Engineering and Sciences*, vol. 1, pp. 19–30.

Chen, S. S.; Liu, Y. H.; Cen, Z. Z. (2008): A combined approach of the MLPG method and nonlinear programming for lower-bound limit analysis. *CMES: Computer Modeling in Engineering and Sciences*, vol. 28, pp. 39–55.

Cocchetti, G.; Maier, G. (2003): Elastic-plastic and limit-state analyses of frames with softening plastic-hinge models by mathematical programming. *International Journal of Solids and Structures*, vol. 40, pp. 7219–7244.

Cocchetti, G.; Maier, G.; Shen, X. P. (2002): Piecewise linear models for interfaces and mixed mode cohesive cracks. *CMES: Computer Modeling in Engineering and Sciences*, vol. 3, pp. 279–298.

Cottle, R. W.; Pang, J. S.; Stone, R. E. (1992): *The Linear Complementarity Problem*. Academic Press, San Diego.

DeDonato, O.; Maier, G. (1972): Mathematical programming methods for the inelastic analysis of reinforced concrete frames allowing for limited rotation capacity. *International Journal for Numerical Methods in Engineering*, vol. 4, pp. 307–329.

DeFreitas, J. A. T.; LloydSmith, D. (1984–85): Elastoplastic analysis of planar structures for large displacements. *Journal of Structural Mechanics*, vol. 12, pp. 419–445.

Dirkse, S. P.; Ferris, M. C. (1995): The PATH solver: A nonmonotone stabilization scheme for mixed complementarity problems. *Optimization Methods and Software*, vol. 5, pp. 123–156.

Drud, A. S. (1994): CONOPT – a large-scale GRG code. *ORSA Journal on Computing*, vol. 6, pp. 207–216.

Ehrlich, D.; Armero, F. (2005): Finite element methods for the analysis of softening plastic hinges in beams and frames. *Computational Mechanics*, vol. 35, pp. 237–264.

Ferris, M. C. (1998): MATLAB and GAMS: Interfacing Optimization and Visualization Software. Technical Report TR98-19, Computer Sciences Department, University of Wisconsin, Madison, Wisconsin, 1998.

Ferris, M. C.; Pang, J. S. (1997): Engineering and economic applications of complementarity problems. *SIAM Review*, vol. 39, pp. 669–713.

Ferris, M. C.; Tin-Loi, F. (1999): On the solution of a minimum weight elastoplastic problem involving displacement and complementarity constraints. *Computer Methods in Applied Mechanics and Engineering*, vol. 174, pp. 107–120.

Ferris, M. C.; Tin-Loi, F. (2001): Limit analysis of frictional block assemblies as a mathematical program with complementarity constraints. *International Journal of Mechanical Sciences*, vol. 43, pp. 209–224.

Franchi, A.; Cohn, M. Z. (1980): Computer analysis for elastic-plastic structures. *Computer Methods in Applied Mechanics and Engineering*, vol. 21, pp. 271–294.

Kamenjarzh, J. A. (1996): *Limit Analysis of Solids and Structures*. CRC Press, Boca Baton.

Kanzow, C. (1996): Some noninterior continuation methods for linear complementarity problems. *SIAM Journal on Matrix Analysis and Applications*, vol. 17, pp. 851–868.

Karakostas, S. M.; Mistakidis, E. S. (2000): Evaluation of the ductility features in steel structures with softening moment-rotation behaviour based on a nonconvex optimization formulation. *Engineering Computations*, vol. 17, pp. 573–592.

Leu, S.-Y.; Chen, J. T. (2006): Sequential limit analysis of rotating hollow cylinders of nonlinear isotropic hardening. *CMES: Computer Modeling in Engineering and Sciences*, vol. 14, pp. 129–140.

Liu, C.-S.; Atluri, S. N. (2008): A fictitious time integration method (FTIM) for solving mixed complementarity problems with applications to non-linear optimization. *CMES: Computer Modeling in Engineering and Sciences*, vol. 34, pp. 155–178.

Long, S. Y.; Liu, K. Y.; Li, G. Y. (2008): An analysis for the elasto-plastic fracture problem by the meshless local Petrov-Galerkin method. *CMES: Computer Modeling in Engineering and Sciences*, vol. 28, pp. 203–216.

Luo, Z. Q.; Pang, J. S.; Ralph, D. (1996): *Mathematical Programs with Equilibrium Constraints*. Cambridge University Press, Cambridge.

Maier, G. (1970): A matrix structural theory of piecewise linear elastoplasticity with interacting yield planes. *Meccanica*, vol. 5, pp. 54–66.

Maier, G. (1971): Incremental plastic analysis in the presence of large displacements and physical instabilizing effects. *International Journal of Solids and Structures*, vol. 7, pp. 345–372.

Maier, G.; Drucker, D. C. (1973): Effects of geometry change on essential features of inelastic behavior. *Journal of the Engineering Mechanics Division (ASCE)*, vol. 99, pp. 819–834.

Maier, G.; Giacomini, S.; Paterlini, F. (1979): Combined elastoplastic and limit analysis via restricted basis linear programming. *Computer Methods in Applied Mechanics and Engineering*, vol. 19, pp. 21–48.

Maier, G.; Zavelani, A.; Dotreppe, J. C. (1973): Equilibrium branching due to flexural softening. *Journal of the Structural Division (ASCE)*, vol. 99, pp. 897–906.

Massonnet, C. E.; Save, M. A. (1965): *Plastic Analysis and Design, Vol 1: Beams and Frames*. Blaisdell Publishing Co, New York.

Przemieniecki, J. S. (1985): *Theory of Matrix Structural Analysis*. Dover Publication Inc, New York.

Tangaramvong, S.; Tin-Loi, F. (2007a): A complementarity approach for elastoplastic analysis of strain softening frames under combined bending and axial force. *Engineering Structures*, vol. 29, pp. 742–753.

Tangaramvong, S.; Tin-Loi, F. (2007b): Limit analysis of strain softening steel frames under pure bending. *Journal of Constructional Steel Research*, vol. 63, pp. 1151–1159.

Tangaramvong, S.; Tin-Loi, F. (2009): Limit analysis of elastoplastic frames considering 2nd-order geometric nonlinearity and displacement constraints. *International Journal of Mechanical Sciences*, vol. 51, pp. 179–191.

Tin-Loi, F. (1999): A smoothing scheme for a minimum weight problem in structural plasticity. *Structural Optimization*, vol. 17, pp. 279–285.

Tin-Loi, F.; Que, N. S. (2002): Nonlinear programming approaches for an inverse problem in quasibrittle fracture. *International Journal of Mechanical Sciences*, vol. 44, pp. 843–858.

Tin-Loi, F.; Tangaramvong, S.; Xia, S. H. (2007): Limit analysis of frames involving unilateral supports with frictional contact. *International Journal of Mechanical Sciences*, vol. 49, pp. 454–465.

Tin-Loi, F.; Tseng, P. (2003): Efficient computation of multiple solutions in quasibrittle fracture analysis. *Computer Methods in Applied Mechanics and Engineering*, vol. 192, pp. 1377–1388.

Tin-Loi, F.; Vimonsatit, V. (1996): Nonlinear analysis of semirigid frames: a parametric complementarity approach. *Engineering Structures*, vol. 18, pp. 115–124.

Tin-Loi, F.; Xia, S. H. (2001): Holonomic softening: Models and analysis. *Mechanics of Structures and Machines*, vol. 29, pp. 65–84.

Tonković, Z.; Sorić, J.; Skozrit, I. (2008): On numerical modeling of cyclic elastoplastic response of shell structures. *CMES: Computer Modeling in Engineering and Sciences*, vol. 26, pp. 75–90.